European Journal of Pharmaceutical Sciences 195 (2024) 106727

Contents lists available at ScienceDirect

European Journal of Pharmaceutical Sciences

journal homepage: www.elsevier.com/locate/ejps

Implementing physics-based digital patient twins to tailor the switch of oral morphine to transdermal fentanyl patches based on patient physiology

Flora Bahrami [a,b], René Michel Rossi [a], Katelijne De Nys [c,d], Markus Joerger [e], Milena Cukic Radenkovic [a], Thijs Defraeye [a,*]

[a] Laboratory for Biomimetic Membranes and Textiles, Empa, Swiss Federal Laboratories for Materials Science and Technology, Lerchenfeldstrasse 5, St. Gallen CH-9014, Switzerland
[b] ARTORG Center for Biomedical Engineering Research, University of Bern, Mittelstrasse 43, Bern CH-3012, Switzerland
[c] Kantonsspital St. Gallen, Palliativzentrum, Rorschacherstrasse 95, St. Gallen CH-9000, Switzerland
[d] Department of Pharmaceutical and Pharmacological Sciences, KU Leuven, ON2 Herestraat 49 - box 424, Leuven BE-3000, Belgium
[e] Kantonsspital St. Gallen, Medizinische Onkologie und Hämatologie, Rorschacherstrasse 95, St. Gallen CH-9000, Switzerland

ARTICLE INFO

Keywords:
Opioid therapy
Pharmacokinetics model
Pharmacodynamics model
Tailored therapy
Virtual population

ABSTRACT

Fentanyl transdermal patches are widely implemented for cancer-induced pain treatment due to the high potency of fentanyl and gradual drug release. However, transdermal fentanyl up-titration for opioid-naïve patients is difficult, which is why opioid treatment is often started with oral/iv morphine. Based on the daily dose of morphine, the initial dose of the fentanyl patch is decided upon. After reaching a stable level of pain, the switch is made from oral/iv morphine to transdermal fentanyl. There are standard calculation tools for transferring from oral/iv morphine to transdermal fentanyl, which is the same for all patients. By considering the variations in the physiology of the patients, a unique switching strategy cannot meet the needs of different patients. This study explores the outcome in terms of pain relief and minute ventilation during opioid therapy. For this, we used physics-based simulations on a virtually-generated population of patients, and we applied the same therapy to all patients. We could show that patients' physiology, such as gender, age, and weight, greatly impact the outcome of the therapy; as such, the correlation coefficient between pain intensity and age is 0.89, and the correlation coefficient between patient's weight and maximum plasma concentration of morphine and fentanyl is -0.98 and -0.97. Additionally, a different combination of the duration of overlap between morphine and fentanyl therapy with different doses of fentanyl was considered for the virtual patients to find the best opioid-switching strategy for each patient. We explored the impact of combining physiological features to determine the best-suited strategy for virtual patients. Our findings suggest that tailoring morphine and fentanyl therapy only based on a limited number of features is insufficient, and increasing the number of impactful physiological features positively influences the outcome of the therapy.

1. Introduction

Pain is a common and critical symptom of cancer (Paice and Ferrell, 2011). 50 % of patients undergoing cancer treatment and 90 % at the advanced stage suffer from cancer-induced pain (Money and Garber, 2018). Uncontrolled pain reduces the patient's quality of life and negatively impacts the physical and psychological condition of the patient (Paice and Ferrell, 2011). Transdermal fentanyl is a potent opioid that is widely used for cancer-induced pain control. Transdermal delivery is a common administration route for fentanyl, which reduces the fluctuation of fentanyl exposure and is practical for patients since the patches only need to be replaced every three days. However, due to the high potency of fentanyl, it is not recommended for opioid-naïve patients. Based on the clinical practices, the patient starts with oral or subcutaneous morphine; after stabilizing the pain relief, the patient switches to fentanyl transdermal therapy. Morphine therapy continues for 12 h alongside the application of the first fentanyl patch (Eastern Metropolitan Region Palliative Care Consortium, 2014), and the patch concentration is determined based on the daily morphine dose (Donner et al., 1996).

Fentanyl is 50 to 100 times more potent than morphine, and its potency is taken to account in switching from oral/iv morphine to

* Corresponding author.
E-mail address: thijs.defraeye@empa.ch (T. Defraeye).

https://doi.org/10.1016/j.ejps.2024.106727
Received 12 July 2023; Received in revised form 20 December 2023; Accepted 12 February 2024
Available online 13 February 2024

transdermal fentanyl (Drug Enforcement Administration DEA, U.S. Department of Justice, 2007). Different tools and guidelines exist for switching from oral or subcutaneous morphine to transdermal fentanyl. Among them, the Opimeter from the University Hospital of Zurich is in common use in Switzerland, the conversion guideline by the Duragesic® label (US Food and Drug Administration, 2005), and equianalgesic dose calculation guidelines by Stanford School of Medicine are in use. These converters and guidelines propose different fentanyl doses based on the daily dose of oral morphine. In these tools, only the prior dose of oral morphine is being considered; even though the suitable oral morphine dose is personalized, it does not include the impact of other physiological features that impact fentanyl transdermal therapy. Skin characteristics significantly impact fentanyl absorption, unlike oral morphine, where daily dosage is unaffected. Renal clearance is the primary elimination factor for morphine and its byproducts, while it has minimal impact on transdermal fentanyl. There are fundamental differences between the factors that impact oral morphine and transdermal fentanyl therapy. Skin characteristics have a huge impact on the intake of fentanyl, while its impact on the daily dose of oral morphine is not reflected. On the other hand, the renal clearance rate acts as the main elimination path for morphine and its metabolites, while its impact is negligible for transdermal fentanyl. Additionally, the enzymes involved in the metabolism of morphine and fentanyl are different. Due to this individual variability in terms of skin thickness, metabolic enzyme activity, renal clearance, etc., the patient's response to oral morphine therapy and fentanyl transdermal therapy may differ (Rennick et al., 2016). Therefore, implementing the same strategy for switching from oral morphine to transdermal fentanyl for all patients is inadequate. By focusing on experimental and clinical studies, some researchers explored the variability in opioid-switching strategies (Bruijn et al., 2018; Corli et al., 2019; Treillet et al., 2018; Jackson et al., 2021; Mercadante et al., 2023). Some studies implemented molecular modeling to study the interaction of the μ-opioid receptor with opioids such as fentanyl, morphine, or heroine and their different activation patterns (Ricarte et al., 2021; Giannos et al., 2021; Podlewska et al., 2020). However, regardless of the importance of inter-individual variability in opioid switching, no study tailors the transfer for individual patients based on their physiological features. Such tailoring is, however, challenging in a clinical setting. The therapeutic window for patients is narrow, as underdosing can put the patient in unbearable discomfort, and overdosing can cause a range of disturbing and potentially dangerous side effects, including but not limited to nausea, dizziness, and respiratory depression. Therefore, *in-silico* experiments using digital twins could support defining the patients' individual therapeutic window.

In this study, we aim to develop a tailored physics-based digital twin to predict the best strategy rotation for each virtual patient. This digital twin includes the Pharmacokinetics (PK) / pharmacodynamics (PD) model for morphine and fentanyl uptake from the skin and the PK/PD model for fentanyl. The tailored physics-based digital twin predicted the outcome of oral morphine followed by transdermal fentanyl therapy on virtual patients, and subsequently, we analyzed the impact of patients' physiological features on therapy outcomes. In the next step, we explored different strategies for switching from oral morphine to transdermal fentanyl by changing the overlap time and the first two fentanyl patch sizes. Based on the outcome of these strategies, the most suited strategy was defined for each virtual patient, and we explored the distribution of physiological features of patients based on this individualized strategy.

2. Materials and methods

2.1. Digital twin of the patients

A digital twin is a virtual representation of a real-world object that contains relevant elements and kinetics and is connected to the object via monitoring tools such as wearable sensors. In this study, a physics-based digital twin is developed for a patient, tailored for each virtual patient based on age, weight, gender, height, serum albumin, serum creatinine, and bilirubin. This digital twin monitor has two sequential therapies, immediate-release oral morphine, and transdermal fentanyl therapy. However, the immediate release form is uncommon in the clinic due to practical problems as they need to be taken every 4 h. It is mainly used as a "reserve/backup" medication for acute pain episodes. This twin contains a pharmacokinetics and pharmacodynamics model for morphine, a mechanistic drug uptake model through the skin for fentanyl and pharmacokinetics, and a pharmacodynamics model for fentanyl. Throughout this study, the conventional SmPC (summary of product characteristics) therapy for immediate-release oral morphine followed by fentanyl transdermal therapy is applied to evaluate the therapy performance for different patients. The general structure of this study is depicted in Fig. 1.

2.1.1. Immediate-release oral morphine

In this study, we assumed that virtual patients take immediate-release oral morphine for 24 h before starting fentanyl transdermal therapy. As mentioned in Section 2.1, immediate-release oral morphine is not the common oral morphine for cancer-induced pain; however, it was chosen in this study due to available data on immediate-release morphine plasma concentration and its metabolites. Additionally, 24 h might be adequate to reach a steady state for immediate-release oral morphine; however, it is not sufficient for adjusting the adequate dose for pain control. Immediate-release oral morphine is prescribed to be used every four hours. In this study, we considered oral morphine with an equivalent dose of 20 mg at each interval (every 4 h). The pharmacokinetics and pharmacodynamics models corresponding to this drug are provided in the following sections.

2.1.1.1. Pharmacokinetic modeling. As the patient takes oral morphine, the drug will be absorbed by the intestine. Therefore, there is a time lag of around half an hour to two hours between the intake of morphine and its absorption into the body. After absorption of morphine via the intestine, it will be transferred to the liver via the hepatic portal vein. In the liver, morphine will be metabolized by a group of enzymes predominantly by UGT2B7 to M6G (Morphine-6-glucuronide) and M3G (Morphine-3-glucuronide) (De Gregori et al., 2012). The remaining morphine and the produced M6G and M3G will be taken up by the venous system and distributed in the body. Here, we considered several compartments that represent organs and tissues in the body for the morphine pharmacokinetics (PK) model, which are described as follows: 1. Morphine depot in the intestine (Eq. (1)); 2. Intestine (Eq. (2)); 3. Arterial system (Eq. (3)); 4. Venous system (Eq. (4)); 5. Blood cells in an artery (Eq. (5)); 6. Lung (German, 2019); 7. Muscle (German, 2019); 8. Adipose (German, 2019); 9. Bone marrow (German, 2019); 10. Spleen (German, 2019); 11. Kidney (Eq. (6)); 12. Residual blood (German, 2019); 13. Residual tissue (German, 2019); 14. Liver (Eq. (7)). These compartments represent the whole body without the central nervous system. The compartments representing the central nervous system are as follows 1. Blood-brain (German, 2019); 2. Brain interstitial fluid (German, 2019); 3. Brain tissue (German, 2019); 4. Spinal cerebrospinal fluid (German, 2019); 5. Cranial cerebrospinal fluid (German, 2019). The general structure of the morphine pharmacokinetic model was developed based on the German et al. study (German, 2019). The overall structure pharmacokinetics model for oral morphine is depicted in Fig. 2.

$$\frac{\partial c_{M,depot}}{\partial t} = -k_{o,M} * c_{M,depot}, \; t = 0s : c^{0}_{M,depot} = 20\ mg \tag{1}$$

$$\frac{\partial c_{M,int}}{\partial t} = Q_{int} * \left(c_{M,art} - \frac{c_{M,int}}{k_{int}} \right) \Big/ v_{int} + k_{o,M} * c_{M,depot} \tag{2}$$

Eqs. (3)–(7) are based on the study conducted by German (2019)

$$\frac{\partial c_{M,art}}{\partial t} = \left(Q_{bl} * c_{M,lun} - \left(Q_{mus} - Q_{adi} - Q_{bon} - Q_{kid} - Q_{res,t} - Q_{liv} - Q_{spl} - Q_{int} - Q_{bra} \right) * c_{M,art} - P_{art,pla} * \left(c_{M,art} - \frac{c_{M,art,cell}}{k_{bl,\ cell}} \right) \right) \Big/ V_{art} \quad (3)$$

$$\frac{\partial c_{M,vei}}{\partial t} = \left(Q_{bra} * C_{BB} + Q_{mus} * \frac{c_{M,mus}}{k_{mus}} + Q_{adi} * \frac{c_{M,adi}}{k_{adi}} + Q_{bone} * \frac{c_{M,bone}}{k_{bone}} + Q_{kid} * \frac{c_{M,kid}}{k_{kid}} + Q_{res,b} * c_{M,res,b} + \left(Q_{liv} + Q_{spl} + Q_{int} \right) * c_{M,liv} \Big/ k_{liv} - Q_{bl} * c_{M,vei} \right) \Big/ v_{vei} \quad (4)$$

$$\frac{\partial c_{M,art,cell}}{\partial t} = P_{art,pla} * \left(c_{M,art} - \frac{c_{M,art,cell}}{k_{bl,\ cell}} \right)) / V_{art,cell} \quad (5)$$

$$\frac{\partial c_{M,kid}}{\partial t} = Q_{kid} * \frac{c_{M,art} - \frac{c_{M,kid}}{k_{kid}}}{v_{kid}} - f_{ut} * c_{M,kid} * Cl_{ren} \quad (6)$$

$$\frac{\partial c_{M,liv}}{\partial t} = \left(Q_{liv} * c_{M,art} + Q_{spl} * \frac{c_{M,spl}}{k_{spl}} + Q_{int} * \frac{c_{M,int}}{k_{int}} - \left(Q_{liv} + Q_{spl} + Q_{int} \right) * \frac{c_{M,liv}}{k_{liv}} \right) \Big/ v_{liv} - f_{ut} * \frac{c_{M,liv}}{v_{liv}} * \left(\frac{V_{m1}}{K_{m1} + f_{ut} * c_{liv}} + \frac{V_{m2}}{K_{m2} + f_{ut} * c_{liv}} + Cl_{nrnh} \right) \quad (7)$$

Where, $c_{M,i}$ [nM] is the concentration of morphine in compartment i and $k_{o,M}$ [min^{-1}] is the absorption constant rate for the immediate release of oral morphine. k_i [min^{-1}] is the partition coefficient of morphine in compartment i, and Q_i [$L.min^{-1}$] is the blood flow to compartment i. V_i [L] is the volume of compartment i, and $p_{art,pla}$ is the permeability rate between plasma and blood cells. f_{ut} is the fraction of unbound morphine in the tissue. V_{m1} [$mol.min^{-1}$], V_{m2} [$mol.min^{-1}$], K_{m1} [M], and K_{m2} [M] are M3G and M6G maximum rate of reaction and M3G and M6G Michaelis–Menten constants, respectively. As morphine metabolizes by the liver, two metabolites M3G and M6G, will be produced. In order to monitor the concentration of these metabolites in the body, we considered one central compartment plus a depot compartment. The concentration of M3G and M6G in the central compartment (equal to the concentration in the plasma) is calculated based on Eqs. (8) and (9), respectively.

$$\frac{\partial c_{M3G}}{\partial t} = f_{ut} * c_{liv} * \left(\frac{V_{m1}}{(K_{m1} + f_{ut} * c_{liv})} \right) - f_{u,M3G} * Cl_{M3G} * \frac{c_{M3G}}{V_{M3G}} \quad (8)$$

$$\frac{\partial c_{M6G}}{\partial t} = f_{ut} * c_{liv} * \left(\frac{V_{m2}}{(K_{m2} + f_{ut} * c_{liv})} \right) - f_{u,M6G} * Cl_{M6G} * \frac{c_{M6G}}{V_{M6G}} \quad (9)$$

Where c_{M3G} [nM] and c_{M6G} [nM] are the concentration of M3G and M6G in the central compartment. $f_{u,i}$ is the fraction of unbound metabolite i in the central compartment.

2.1.1.2. Pharmacodynamics model. There is a time delay between the drug response and the corresponding drug concentration in plasma. A virtual compartment as an effect compartment is considered to capture

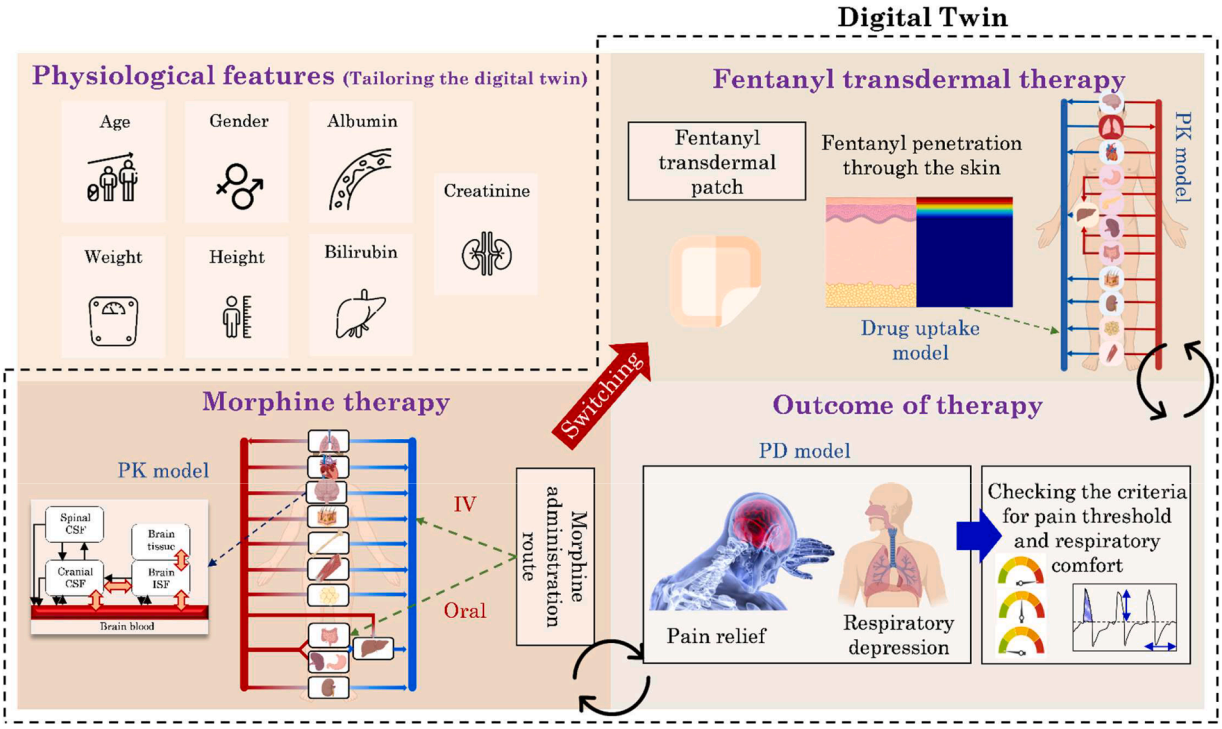

Fig. 1. Overall structure of tailored physics-based digital twin to monitor and modify the switching strategy from oral morphine to fentanyl transdermal patch (Created with BioRender.com and the first block's icons and the patch are from https://www.flaticon.com).

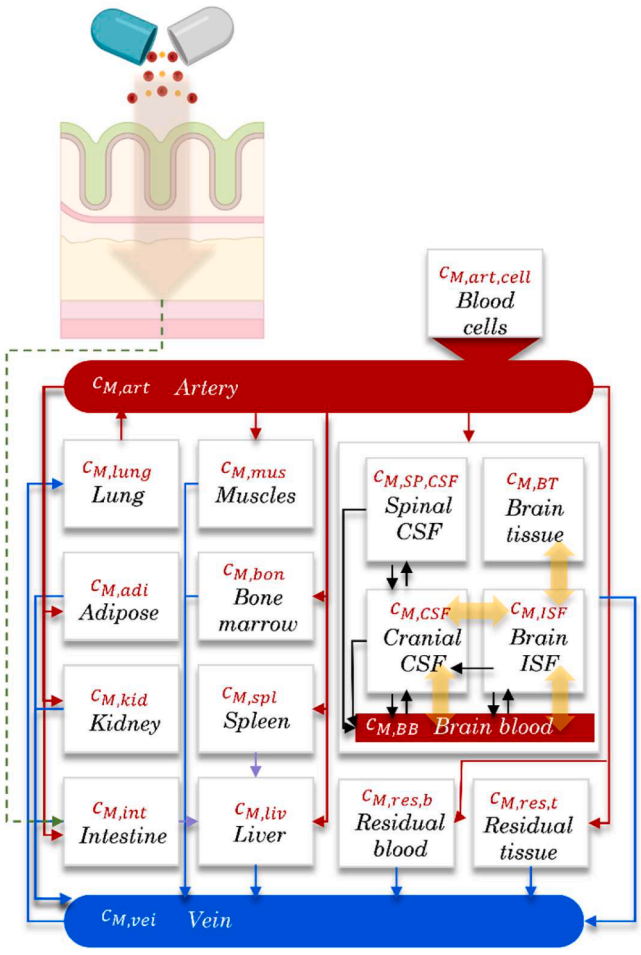

Fig. 2. Physiological-based pharmacokinetics model for immediate-release oral morphine (Created with BioRender.com).

this delay. The effect compartment is different for each substance and each effect. The concentration of the substance in the effect compartment is calculated based on Eq. (10) (Felmlee et al., 2012).

$$\frac{\partial c_{e,i}}{\partial t} = k_{e,i} * \left(c_{plasma,i} - c_{e,i}\right) \tag{10}$$

Where c_i [nM] is the concentration of morphine, or M6G, or M3G in the effect compartment. $k_{e,i}$ [min^{-1}]is the constant equilibrium rate for the substance i and for effect e. Based on the calculated concentration of the substance in the effect compartment, the corresponding effect can be calculated at each time step; for this calculation, we use E_{max} model. Based on Maziot's study, the pain effect as a result of the analgesic effect of morphine and M6G and the anti-analgesic effect of M3G is calculated based on the Gaddum formula in Eq. (11) (Mazoit et al., 2007).

$$E_{pain} = E_{0,pain}\ (1 - \frac{\left(\frac{c_{ep,\ mor}}{IC_{50,p,\ mor}}\right)^{\gamma_{pm}} + \left(\frac{c_{ep,M6G}}{IC_{50,p,\ M6G}}\right)^{\gamma_{pm}}}{1 + \left(\frac{c_{ep,\ M3G}}{IC_{50,p,M3G}}\right)^{\gamma_{pm}} + \left(\frac{c_{ep,\ mor}}{IC_{50,p,\ mor}}\right)^{\gamma_{pm}} + \left(\frac{c_{ep,M6G}}{IC_{50,p,\ M6G}}\right)^{\gamma_{pm}}}) \tag{11}$$

Where E_{pain} and $E_{0,pain}$ is the pharmacologic and baseline effect for pain intensity, respectively. $c_{ep,i}$ and $IC_{50,p,\ i}$ [nM] are the concentration of the substance i in the pain effect compartment, and the concentration of half maximum pain effect corresponds to the substance i, and γ_{pm} is the Hill coefficient for the pain effect model. To our best knowledge, there is no impact of M3G on the patient's minute ventilation, so the presence of M3G in the body would not increase or decrease the patient's minute ventilation. Therefore, the minute ventilation at each time step is only calculated here based on the concentration of morphine and M6G, and the term related to the impact of M3G is removed.

$$E_{vent} = E_{0,vent}\ (1 - \frac{\left(\frac{c_{ev,\ mor}}{IC_{50,v,\ mor}}\right)^{\gamma_{vm}} + \left(\frac{c_{ev,M6G}}{IC_{50,v,\ M6G}}\right)^{\gamma_{vm}}}{1 + \left(\frac{c_{ev,\ mor}}{IC_{50,v,\ mor}}\right)^{\gamma_{vm}} + \left(\frac{c_{ev,M6G}}{IC_{50,v,\ M6G}}\right)^{\gamma_{vm}}}) \tag{12}$$

Here, E_{vent} and $E_{0,vent}$ are pharmacologic ($L.min^{-1}$) and baseline minute-ventilation effects [$L.min^{-1}$]. $c_{ev,i}$ and $IC_{50,v,i}$ are the concentration of substance i in the minute-ventilation effect compartment and half maximum minute-ventilation reduction effect corresponded to substance i, respectively.

2.1.2. Fentanyl transdermal therapy

As transdermal fentanyl is not frequently prescribed for opioid-naïve patients, opioid treatment is usually started with oral/iv morphine; based on the daily oral morphine dose, the suitable size of the fentanyl patch is chosen. In order to cover the time lag in fentanyl transdermal therapy, morphine therapy continues 12 h after applying the first patch of fentanyl. The following sections describe the drug uptake, pharmacokinetics, and pharmacodynamics of fentanyl.

2.1.2.1. Drug uptake model. As the fentanyl transdermal patch is applied to the skin, the fentanyl will penetrate into the skin and eventually will be uptaken by the blood circulation system. A detailed model of fentanyl drug uptake by the skin is provided in our previous studies (Bahrami et al., 2023, 2022; Defraeye et al., 2020, 2021). The general geometry of the drug uptake model coupled with the pharmacokinetic model of fentanyl is depicted in Fig. 3.

2.1.2.1.1. Computational system configuration.

2.1.2.1.2. The governing equation. Fick's second law is used to model the penetration of fentanyl from the patch into the skin until it is absorbed into the bloodstream (Eq. (13))(Manitz et al., 1998). However, as a result of different hydrophobicity in different layers, the dissolubility of fentanyl is different in each layer. As a result, the concentration of fentanyl in the interface of the two layers is different, which can be computationally expensive and unstable. Therefore, we used the drug potential ψ, which is continuous throughout the geometry and defined as $c_i = (k_i/k_j)\ \psi_i = K_{i/j}\ \psi_i$. k_i is the drug capacity in domain *i*, and $K_{i/j}$ is the partition coefficient at the interface of domain *i* and *j*.

$$\frac{\partial c_{F,i}}{\partial t} = -\nabla . j_{F,i} = \nabla . \left(D_i \nabla c_{F,i}\right) \tag{13}$$

Where $c_{F,i}$ [$ng.ml^{-1}$], $j_{F,I}$ [$mg.ml^{-1}.s^{-1}$], and D_i [$m.s^{-2}$] are the fentanyl concentration, fentanyl flux, and diffusion coefficient of fentanyl in domain *i*, respectively.

2.1.2.1.3. Boundary and initial conditions. Before applying the fentanyl patch, we assumed that the concentration of fentanyl in skin layers was zero. This implies that the patch is applied to a skin site where no fentanyl patch had been placed previously. As depicted in Fig. 3a, we assumed no fentanyl flux in the upper and peripheral boundaries; however, the bottom boundary has the fentanyl concentration as same as fentanyl concentration in plasma. Through the bottom boundary, the fentanyl is absorbed by blood circulation.

2.1.2.2. Pharmacokinetics modeling. Blood circulation distributes fentanyl throughout the body, which will be metabolized in the liver by Cytochrome P450. In order to calculate the concentration of fentanyl in the body by including the distribution, metabolism, and elimination, we used a lumped approach for the physiologically based pharmacokinetic

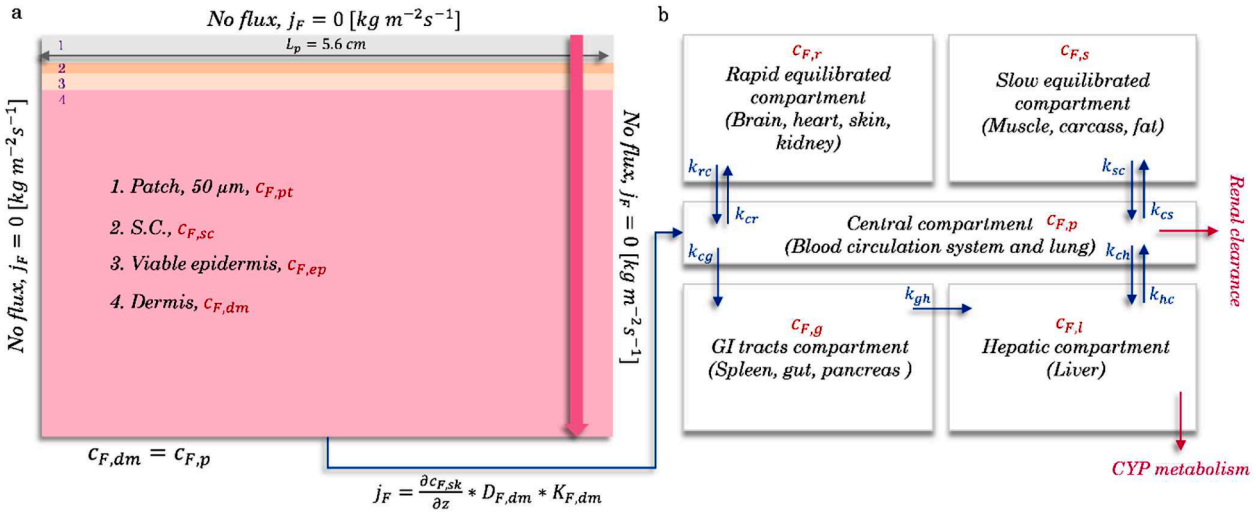

Fig. 3. a: Overall structure of the drug uptake model, including a transdermal patch, stratum corneum, viable epidermis, and dermis; b: compartment model of pharmacokinetics model for fentanyl.

model chosen, as it is shown in Fig. 3b. In this model, we considered five compartments: 1. Central compartment (Eq. (14)), which includes the blood circulation system and lungs; 2. Rapid equilibrated compartment (Eq. (15)) lumped brain, heart, skin, and kidneys; 3. The slow equilibrated compartment (Eq. (16)) represents muscles, carcass, and adipose tissue; 4. The GI tract compartment (Eq. (17)) includes the spleen, gut, and pancreas; and lastly, 5. The hepatic compartment (Eq. (18)) captures the CYP metabolism of fentanyl in the liver.

$$\frac{\partial c_{F,p}}{\partial t} = flux_F \times \frac{A}{V_c} - \left(k_{cs} + k_{cr} + k_{cl} + k_g - k_{re}\right) \times f_{u,F} \times c_{F,p} + k_{rc} \times c_{F,r} + k_{sc} \times c_{F,s} + k_{hc} \times c_{F,l} \tag{14}$$

$$\frac{\partial c_{F,r}}{\partial t} = k_{cr} \times c_{F,p} - k_{rc} \times c_{F,r} \tag{15}$$

$$\frac{\partial c_{F,s}}{\partial t} = k_{cs} \times c_{F,p} - k_{sc} \times c_{F,s} \tag{16}$$

$$\frac{\partial c_{F,g}}{\partial t} = k_{cg} \times c_{F,p} - k_{gl} \times c_{F,g} \tag{17}$$

$$\frac{\partial c_{F,l}}{\partial t} = k_{cl} \times c_{F,p} - k_{lc} \times c_{F,l} + k_{gl} \times c_{F,g} - k_{met} \times c_{F,l} \tag{18}$$

Where $c_{F,i}$[ng.ml^{-1}], and $k_{i,j}$ [min^{-1}]are the concentration of fentanyl in compartment i and the first-order equilibrium rate constant from compartment i to j. $flux_F$ is the flux of fentanyl from the dermis layer to the blood circulation. A and V_c are the surface area between the dermis and blood circulation at the absorption site and the volume of the central compartment. $f_{u,F}$ corresponds to the fraction of unbound fentanyl in the plasma.

2.1.2.3. Pharmacodynamics model. As mentioned in Section 2.1.1.2, there is a time delay between a rise in fentanyl concentration in plasma and the corresponding effect on pain relief. This delay is implemented by considering a virtual compartment as an effect compartment. The concentration of fentanyl in the effect compartment is calculated based on Eq. (19) (Yassen et al., 2007). The corresponding effect for the calculated fentanyl concentration in the effect compartment is based on E_{max} model (Eq. (20))(Yassen et al., 2007).

$$\frac{\partial c_{e,F}}{\partial t} = k_{e,F} * \left(c_{F,p} - c_{e,F}\right) \tag{19}$$

$$E_i = E_{0,i}\left(1 - \frac{\left(\frac{c_{e,F}}{IC_{50,e,\ F}}\right)^{\gamma_{eF}}}{1 + \left(\frac{c_{e,F}}{IC_{50,e,\ F}}\right)^{\gamma_{eF}}}\right) \tag{20}$$

Where $c_{e,F}$ [ng.ml^{-1}], and $k_{e,F}$ [min^{-1}] are the concentration of fentanyl in effect compartment e, and the first-order equilibrium rate constant for effect e. γ_{eF} is the Hill coefficient of fentanyl for effect e. E_i, $E_{0,i}$, and $IC_{50,e,\ F}$ [ng.ml^{-1}] are pharmacologic effects, baseline effects, and concentrations of half maximum of effect e. However, as fentanyl transdermal therapy starts, morphine therapy continues alongside it for a while. Therefore the effect of pain intensity and minute ventilation should be the result of their combination. For simplicity, we assumed the combination of morphine, its metabolites, and fentanyl is additive; therefore, the effect model will be as follows (Eq. (21))(Bisaso et al., 2022).

$$E_{i,t} = E_{0,i} - E^*_{i,M} - E^*_{i,F} + E^*_{i,M}\ E^*_{i,F} \tag{21}$$

Where $E_{i,t}$ and $E_{0,i}$ are the total pharmacological and baseline for effect i. $E^*_{i,M}$ and $E^*_{i,F}$ are the impact of morphine and its metabolites, and fentanyl in the changes in the baseline of effect i (pain relief or reduction in minute-ventilation).

2.2. Generation of the virtual population

2.2.1. Participants- sample data

As a basis for this work, we used the data that KSSG (local St. Gallen Hospital) kindly shared with us to re-use since they regularly collect the data on patients who are put on fentanyl treatment. All the procedures applied at KSSG fentanyl treatment were in line with the ethical standards of the institutional and/or national research committee and with the 1964 Helsinki Declaration and its later amendments or comparable ethical standards. Since it was not a formal study/project data collection but just for clinical follow-up, we used a standard form of Informed Patients Consent Document (attached as annex data to this manuscript), approved by the local Ethical Committee (St. Gallen, Switzerland). The original sample (from which we later made a virtual patient sample, see in Section 2.2.2) comprised eight patients (we did not know their identity nor any relatable personal data since the KSSG database was already anonymized) aged between 43 and 85 years old, with an average 67.6±13.4 years), all of the inpatients of palliative care department at KSSG (with whom Empa Institute has a written Collaboration Agreement, as one of the main research partners). All the participants were

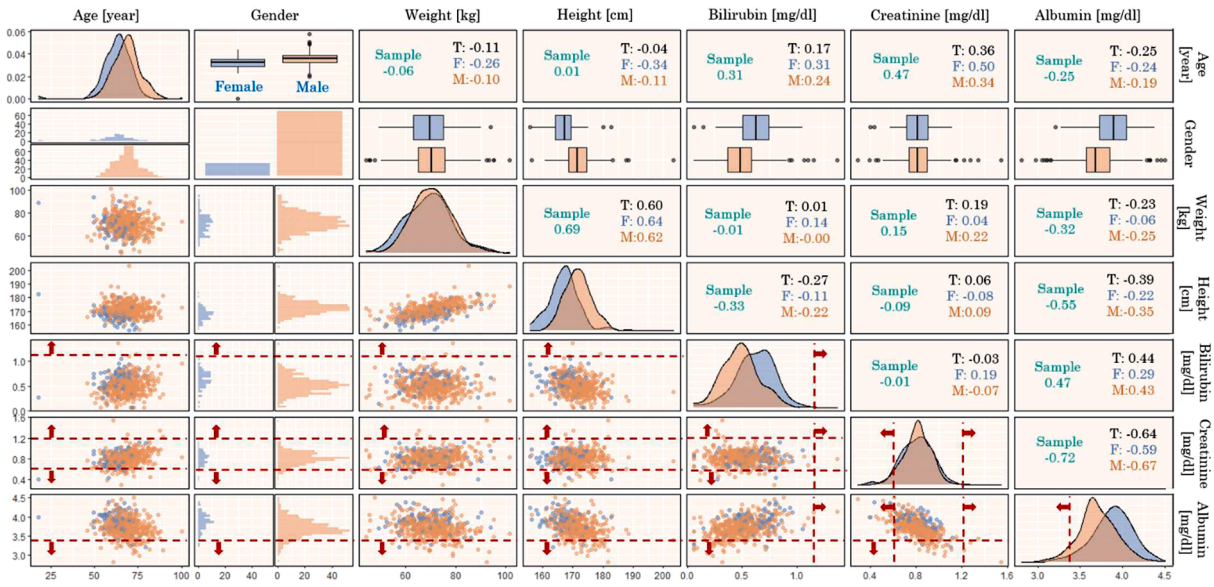

Fig. 4. Distribution and corresponding correlation coefficient of physiological features of generated population based on the sample data.

informed about the clinical protocol and signed informed consent forms. Other than the age of any particular participant, we used their weight (52.6–90 [kg], 70.3±13.6[kg]) and height (154–182[cm], 171.25±8.9 [cm]) information, but also plasma concentrations of bilirubin (0.18–1.05[mg/dl], 0.51±0.32[mg/dl]), albumin (2.96–4.43 [g/dl], 3.73±0.4[g/dl]), and creatinine (0.58–1.22 [mg/dl], 0.81–0.22 [mg/dl]), previously used for standard clinical checkups and known to be important in uptake and metabolization of fentanyl, important for this work.

2.2.2. Virtual population

In order to study a wider range of characteristics and different combinations, we used Markov chain Monte Carlo (MCMC) to generate a virtual population based on information provided from the sample data. The detail of implemented MCMC method for generating a virtual population is provided in our previous study. Fig. 4 shows the distribution of each characteristic for the 500 members of the virtual population based on gender and the correlation coefficient between every two characteristics. Using MCMC, the correlation coefficient's intensity in the virtual population is similar to the sample data. Based on this data, there is a strong correlation between the weight and height of the patient and between the serum creatinine and serum albumin for the virtual patients.

2.2.3. Estimation of model parameter

In order to tailor the digital twin for each individual, we implemented the impact of these physiological features on the model parameters for morphine, its metabolites, and fentanyl. For example, with increasing age, the thickness of the stratum corneum increases, and the concentration of the half-maximum effect of morphine and fentanyl for pain relief reduces. The details of these tailored parameters and their values for morphine and its metabolites are provided in Table 1. The parameters implemented in the drug uptake, PK, and PD model for fentanyl and their modification based on patients' physiology are brought in Table 2.

2.3. Spatial and temporal discretization

The grid sensitivity analysis by using Richardson extrapolation was done for the diffusion of fentanyl by the Fickian model over the skin layers and fentanyl patch based on the flux out of the dermis, in which spatial discretization error was considered 0.1 %. Based on the grid sensitivity analysis result, quadrilateral grids vary from case to case as the thickness of the skin's layer differs between cases. In some cases, ten quadrilateral cells were sufficient; for some cases, 1500 cells were needed. In order to increase numerical accuracy, the accumulation of grids near the interfaces is higher. An adaptive time step with a maximal value of 1 h was used. Results were also reported at 1 h intervals.

2.4. Numerical implementation and simulation

COMSOL Multiphysics version 6 was used in this study to solve the diffusion process of fentanyl from the patch through the skin in the mechanistic model, the distribution of fentanyl in the human body in the pharmacokinetics model, drug's effect in the pharmacodynamics model. We implemented the MUMPS (MUltifrontal Massively Parallel sparse direct Solver) solver scheme in our simulation. A partial differential equation (PDE) solved the diffusion process of fentanyl in the mechanistic model by a partial differential equation (PDE) interface. To take into account the absorption, distribution, elimination, and metabolization of morphine and fentanyl, the ordinary differential equation (ODE) was used. In the pharmacodynamics model for morphine, based on the calculated morphine and its metabolites in the body by ODE interface, their concentration in effect compartments was calculated. As well as for fentanyl, the concentration of fentanyl in the effect compartment was calculated by the ODE interface. The drug's effect was calculated based on the compound concentration in the effect compartment. The optimization to find the optimum effect parameter for morphine was done in COMSOL by the Levenberg-Marquardt solver. To apply the changes and taken dose, the event interface was used. The population generation was done in RStudio by using the "mixAK" package. Analyzing the sample data, calculating the posterior distribution, generating the virtual patients' characteristics, calculating the model parameters, and analyzing the result of digital twins are done in RStudio.

2.5. Explored opioid-switching strategies

Based on clinical practice, after morphine therapy stabilizes the patient's condition based on pain intensity, the oral morphine therapy switches to fentanyl transdermal therapy. After applying the first fentanyl patch, the immediate-release oral morphine continues for 12 h. In the first part of the study, we considered the recommended 12 h of overlap of oral morphine and fentanyl therapy; however, we explored 0,

Table 1
The tailored parameters for morphine and its metabolites used in PK and PD model.

Model	Symbol	Definition	Value/Equation	Condition	Refs.
Pharmacokinetics model	$k_{0,M}$	absorption constant rate	2 $[1/h]$	–	*Juul et al. (2016), Oosten et al. (2017)
	$c^0_{M,\ depot}$	Morphine dose	20 $[mg]$	–	–
	v_{art}	Volume blood in the artery	$(Weight/70)*1.93[L]$	–	German (2019)
	v_{vei}	Volume blood in the vein	$(Weight/70)*3.855[L]$	–	German (2019)
	v_{lun}	Volume of lung	$(Weight/70)*1.25[L]$	–	German (2019)
	v_{bra}	Volume of brain	$(Weight/70)*1.553[L]$	–	German (2019)
	v_{mus}	Volume of muscles	$(Weight/70)*32.18[L]$	–	German (2019)
	v_{adi}	Volume of adipose tissue	$(Weight/70)*10.72[L]$	–	German (2019)
	v_{bon}	Volume of bone marrow	$(Weight/70)*9.3[L]$	–	German (2019)
	v_{kid}	Volume of kidney	$(Weight/70)*0.33[L]$	–	German (2019)
	v_{liv}	Volume of liver	$(Weight/70)*1.81[L]$	–	German (2019)
	v_{spl}	Volume of spleen	$(Weight/70)*0.2[L]$	–	German (2019)
	v_{int}	Volume of intestine	$(Weight/70)*1.77[L]$	–	German (2019)
	$v_{bl,\ cell}$	Volume of blood cells	$(Weight/70)*1.02[L]$	–	German (2019)
	$v_{res,b}$	Volume of residual blood	$(Weight/70)*0.29[L]$	–	German (2019)
	$v_{res,t}$	Volume of residual tissue	$(Weight/70)*5.5[L]$	–	German (2019)
	q_{art}	Blood flow in the artery	$(Weight/70)*5.325[L/min]$	–	German (2019)
	q_{vein}	Blood flow in the vein	$(Weight/70)*5.325[L/min]$	–	German (2019)
	q_{lun}	Blood flow to the lung	$(Weight/70)*5.325[L/min]$	–	German (2019)
	q_{bra}	Blood flow to the brain	$(Weight/70)*0.64[L/min]$	–	German (2019)
	q_{mus}	Blood flow to muscles	$(Weight/70)*0.905[L/min]$	–	German (2019)
	q_{adi}	Blood flow to adipose tissue	$(Weight/70)*0.266[L/min]$	–	German (2019)
	q_{bon}	Blood flow to bone marrow	$(Weight/70)*0.266[L/min]$	–	German (2019)
	q_{kid}	Blood flow to the kidney	$(Weight/70)*1.012[L/min]$	–	German (2019)
	q_{liv}	Blood flow to the liver	$(Weight/70)*0.346[L/min]$	–	German (2019)
	q_{spl}	Blood flow to the spleen	$(Weight/70)*0.1065[L/min]$	–	German (2019)
	q_{int}	Blood flow to the intestine	$(Weight/70)*0.799[L/min]$	–	German (2019)
	q_{res}	Blood flow to residual tissue	$(Weight/70)*0.985[L/min]$	–	German (2019)
	$P_{art,pla}$	Permeability-surface area plasma to blood cells	$(Weight/70)*(1/60)\ [L/min]$	–	German (2019)
	Cl_{nrnh}	Nonrenal- nonhepatic clearance	$(Weight/70)*(17.976/60)[L/min]$	–	German (2019)
	V_{m1}		$(Weight/70)*0.001[mol/min]$	–	German (2019)
	K_{m1}	Michaelis-Menten constant for morphine to M3G	$0.11[mM]$	–	German (2019)
	V_{m2}		$(Weight/70)*0.0002[mol/min]$	–	German (2019)
	K_{m2}	Michaelis-Menten constant for morphine to M6G	$0.11[mM]$	–	German (2019)
	Cl_{m6g}	Central clearance for M6G	$(Weight/70)*4.23*GFR\hat{}0.78[ml/\text{min}]$	Modified	Oosten et al. (2017), Pauli-Magnus et al. (1999)
	Cl_{m3g}	Central clearance for M3G	$(Weight/70)*4.23*GFR\hat{}0.78[ml/\text{min}]$	Modified	Oosten et al. (2017), Pauli-Magnus et al. (1999)
	v_{M6G}	Volume of central compartment for M6G	$v_{vei}+v_{art}+v_{res,b}+kp_{met}*(v_{liv}+v_{lun}+v_{kid}+v_{bon}+v_{mus}+v_{adi})$	–	–
	v_{M3G}	Volume of central compartment for M3G	$v_{vei}+v_{art}+v_{res,b}+kp_{met}*(v_{liv}+v_{lun}+v_{kid}+v_{bon}+v_{mus}+v_{adi})$	–	–
	kp_{met}	Partition coefficient for morphine metabolites (M6G & M3G)	0.3	–	Imaoka et al. (2021)
	$f_{u,M6G}$	Fraction of unbound M6G	0.9	–	Doherty et al. (2006)
	$f_{u,M3G}$	Fraction of unbound M3G	0.9	–	Doherty et al. (2006)

(*continued on next page*)

Table 1 (*continued*)

Model	Symbol	Definition	Value/Equation	Condition	Refs.
	f_{ut}	Fraction of unbound morphine in tissue	0.045	–	German (2019)
Pharmacodynamics model	$k_{e,p,mor}$	first-order equilibrium rate constant of morphine for the pain relief effect	0.41[1 /*h*]	–	Martini et al. (2011)
	$k_{e,p,M6G}$	first-order equilibrium rate constant of M6G for the pain relief effect	0.23[1 /*h*]	–	Martini et al. (2011)
	$k_{e,p,M3G}$	first-order equilibrium rate constant of M3G for the pain relief effect	0.23[1 /*h*]	–	Martini et al. (2011)
	$IC_{50,p,mor}$	Concentration of half-maximum effect of morphine for the pain relief	$(1 + Gender * 0.1) * (-1.44 * Age + 205.84)$ [*nM*]	Modified	Macintyre and Jarvis (1996), Periasamy et al. (2014)
	$IC_{50,p,M6G}$	Concentration of half-maximum effect of M6G for the pain relief	$(1 + Gender * 0.1) * (-0.15 * Age + 27.72)$[*nM*]	Modified	Macintyre and Jarvis (1996), Periasamy et al. (2014)
	$IC_{50,p,M3G}$	Concentration of half-maximum effect of M3G for the pain relief	111.59[*nM*]	–	–
	γ_{pm}	Hill coefficient for the pain relief	1	–	–
	$k_{e,v,M6G}$	first-order equilibrium rate constant of morphine for the reduction in minute ventilation effect	0.26[1 /*h*]	–	Martini et al. (2011)
	$k_{e,v,mor}$	first-order equilibrium rate constant of M6G for the reduction in minute ventilation effect	0.58[1 /*h*]	–	Martini et al. (2011)
	$IC_{50,v,M6G}$	Concentration of half-maximum effect of morphine for the reduction in minute ventilation	880[*nM*]	–	Martini et al. (2011)
	$IC_{50,v,mor}$	Concentration of half-maximum effect of M6G for the reduction in minute ventilation	160[*nM*]	–	Martini et al. (2011)
	γ_{vm}	Hill coefficient for the reduction in minute ventilation	1	–	–

*The valuse is chosen in the range of provided referrences.

12, and 24 h of overlap for the later part of the study. This implies that we terminated the morphine therapy at 24 h, 36 h, and 48 h from the start of the treatment. The fentanyl patch size is determined based on the oral morphine in the last 24 h. There are different methods to determine the patch size, which calculates based on the fentanyl potency compared to morphine will recommend a higher dose for fentanyl compared to the recommendation of Duragesic® label (US Food and Drug Administration, 2005). In this study, for the immediate release of oral morphine, we considered 20 mg of morphine every 4 h, equal to 180 mg of morphine per day. Therefore, considering the fentanyl potency, by equianalgesic dose calculation guidelines by the Stanford School of Medicine, the suitable fentanyl patch has a flux of 50 μg/h. However, the Opimetere recommendation is a patch with a flux of 33.3 μg/h, which is the closest fentanyl patch for it is 37.5 μg/h. For the first part of the study, in order to explore the inter-individual variability in therapy, we considered the fentanyl patch with a nominal flux of 50 μg/h. Later in the study, we explored the outcome of therapy for different strategies that are provided in Table 3 below.

These 12 strategies were applied to each individual in the virtual population, and they were ranked based on the key outcomes. These key outcomes were pain intensity, fentanyl concentration in plasma, and minute ventilation. For each virtual patient, the strategy with the lowest pain intensity received the higher ranks, and as the pain intensity increased, the ranks would drop; however, the rate of reduction in the rank increases when the pain intensity passes 3. Strategies that led to maximum fentanyl concentration in plasma below 2 ng/ml received the highest rank, and as the c_{max} passes 2 ng/ml, by the increase in c_{max} the rank drops. Additionally, the strategies that the minimum minute ventilation in the normal range of 4–8 L/min received higher rank, and as the minimum minute ventilation passes 8 L/min the rank drops; however, when the minimum minute ventilation goes below 4 L/min the strategy received the lowest rank.

2.6. Sensitivity analysis of the physiological features

The sensitivity of minimum pain intensity experienced by virtual patients with physiological features based on the population average to each physiological feature were studied. The virtual patient chosen for the sensitivity analysis is 67.6 years old, male, with body mass of 70.2 kg and height of 171 cm. the serum albumin, creatinine and albumin for this virtual patient is 0.51 mg/dl, 0.81 mg/dl, and 3.73 g/dl, respectively. We divided the duration of therapy in three parts, oral morphine therapy, the first fentanyl patch which for 12 h overlaps with oral morphine therapy, and the second fentanyl patch. The nominal flux of both fentanyl patches was 50 μg/h and the dose of oral morphine was 20 mg per intake. The sensitivity index of minimum pain intensity during each of these three time sections was calculated by Eq. (22).

$$SI_i = \frac{U_{x_i+1} - U_{x_i-1}}{\Delta x_i} \frac{x_i}{U_{x_i}} \tag{22}$$

Where SI_i is the sensitivity index, x_i is the value of physiological features and U_{xi} is the corresponding minimum pain intensity for the physiological feature in study. Here the $\Delta x_i/x_i$ was considered to be 1 %.

3. Results and discussion

3.1. Validation of pharmacokinetics model for morphine

The result of the developed pharmacokinetic model for morphine and its metabolites were validated based on the Bochner et al. study (Bochner et al., 1999). In Bochner et al. study, 24 healthy volunteers were chosen. These volunteers were 18 to 38 years old and weighed 50 to 82 kg. The volunteers were 15 males and nine nonpregnant females who had normal renal, hepatic, and bone marrow function and cardiography. They consumed no alcohol or xanthine-containing products for 48 h before the experiments. For immediate-release oral morphine, they took one dose of 30 mg (30.9 mg) of morphine 'DAK' (Nycomed Denmark A/S, Denmark). Based on the pharmacokinetic model

Table 2
The parameters for fentanyl used in drug uptake, PK, and PD model.

Model	Symbol	Definition	Value/Equation	Condition	Refs.
Drug uptake model	d_{pt}	Thickness of the patch	50.8 $[\mu m]$	–	Rim et al. (2005)
	d_{sc}	Thickness of the stratum corneum	$(0.125\ Age + 11.80\ (Gender + (1 - Gender) * 1.40))\ [\mu m]$	Modified	Boireau-Adamezyk et al. (2014), Firooz et al. (2017)
	d_{ep}	Thickness of viable epidermis	$35.6 * \left(Gender + \frac{1 - Gender}{1.11}\right)\ [\mu m]$	–	Firooz et al. (2017)
	d_{dm}	Thickness of dermis (an equivalent thickness of the dermis)	$\left((Gender * (5.5 * BMI + 143.0) + (1 - Gender) * (4.9 * BMI + 133.7)) * \frac{-2.25 * Age + 354.5}{253}\right)\ [\mu m]$	Modified	Derraik et al. (2014), Firooz et al. (2017), Robert et al. (2012)
	D_{pt}	Diffusion coefficient in patch	$7.03 * 10^{-16} [m^2/s]$	–	Defraeye et al. (2021)
	D_{sc}	Diffusion coefficient in stratum corneum	$3.0 * 10^{-14} [m^2/s]$	–	Defraeye et al. (2021)
	D_{ep}	Diffusion coefficient in the viable epidermis	$3.0 * 10^{-14} [m^2/s]$	–	Defraeye et al. (2021)
	D_{dm}	Diffusion coefficient in the dermis	$3.818 * 10^{-11} [m^2/s]$	–	Holmberg et al. (2008)
	$k_{pt/sc}$	Partition coefficient between patch and stratum corneum	$\frac{1}{3.4}$	–	Defraeye et al. (2021)
	$k_{sc/ep}$	Partition coefficient between stratum corneum and viable epidermis	1	–	Defraeye et al. (2020)
	$k_{ep/dm}$	Partition coefficient between viable epidermis and dermis	1	–	Bahrami et al. (2022)
	L_{patch}	Width of the patch	*Varried*	–	US Food and Drug Administration (2005)
Pharmacokinetics model	V_c	Volume of the central compartment	$(Weight/70) * 23.8[L]$	–	Björkman (2003)
	V_r	Volume of the rapid-equilibrated compartment	$(Weight/70) * 24.5[L]$	–	Björkman (2003)
	V_s	Volume of the slow-equilibrated compartment	$(Weight/70) * 808[L]$	–	Björkman (2003)
	V_g	Volume of GI-tract compartment	$(Weight/70) * 17.3[L]$	–	Björkman (2003)
	V_{liver}	Volume of the hepatic compartment	$(Weight/70) * 20.4[L]$	–	Björkman (2003)
	$Q_{c/r}$	Blood flow from central to rapid-equilibrated compartment	$(Weight/70) * 1.7[L/min]$	–	Bjorkman et al. (1998)
	$Q_{c/s}$	Blood flow from central to slow-equilibrated compartment	$(Weight/70) * 2.2[L/min]$	–	Bjorkman et al. (1998)
	$Q_{c/g}$	Blood flow from central to GI-tract compartment	$(Weight/70) * 0.73[L/min]$	–	Bjorkman et al. (1998)
	$Q_{c/l}$	Blood flow from central to hepatic compartment	$(Weight/70) * 0.175[L/min]$	–	Bjorkman et al. (1998)
	k_{cr}	First-order equilibrium rate constant from central to rapid-equilibrated compartment	$Q_{c/r}/V_c$	–	–
	k_{rc}	First-order equilibrium rate constant from rapid-equilibrated to the central compartment	$Q_{c/r}/V_r$	–	–
	k_{cs}	First-order equilibrium rate constant from central to slow-equilibrated compartment	$Q_{c/s}/V_c$	–	–
	k_{sc}	First-order equilibrium rate constant from slow-equilibrated to the central compartment	$Q_{c/s}/V_s$	–	–
	k_{cg}	First-order equilibrium rate constant from	$Q_{c/g}/V_c$	–	–

(*continued on next page*)

Table 2 (*continued*)

Model	Symbol	Definition	Value/Equation	Condition	Refs.
		central to GI-tract compartment			
	k_{gl}	First-order equilibrium rate constant from GI-tract to hepatic compartment	$Q_{c/g}/V_g$	–	–
	k_{cl}	First-order equilibrium rate constant from central to hepatic compartment	$Q_{c/l}/V_c$	–	–
	k_{lc}	First-order equilibrium rate constant from hepatic to the central compartment	$Q_{c/l}/V_{liver}$	–	–
	$f_{u,F}$	Fraction of unbound fentanyl	0.17	–	Miller et al. (1997)
	k_{re}	First-order equilibrium rate constant for renal clearance	$(Weight/70) * 0.037/V_c$ [1/*min*]	–	Encinas et al. (2013)
	k_{met}*	First-order equilibrium rate constant for metabolism	$(Weight/70) * CYP_{activity} * (1+(1-Gender) * 0.16) * 0.88/f_{u,F}$ /V_liver [1/*min*]	Modified	Encinas et al. (2013)
Pharmacodynamics model	$k_{e,v,F}$	first-order equilibrium rate constant of fentanyl for the reduction in minute ventilation effect	0.0422 [1/*min*]	–	Yassen et al. (2007)
	γ_{vF}	Hill coefficient for the reduction in minute ventilation	2.68	–	Yassen et al. (2007)
	$IC_{50,v,F}$	Concentration of half-maximum effect of fentanyl for the reduction in minute ventilation	1140 [*ng*/*L*]	–	Yassen et al. (2007)
	$k_{e,p,F}$	first-order equilibrium rate constant of fentanyl for the pain relief effect	0.31 [1/*min*]	–	Encinas et al. (2013)
	γ_{pF}	Hill coefficient for pain relief	2.7	–	Sandler et al. (1992)
	$IC_{50,p,F}$	Concentration of half-maximum effect of fentanyl for pain relief	$(-1.148 * 10^{-2} * Age + 1.96)[ng/ml]$	–	Sandler et al. (1992)

*The child-pugh score was calculated based on serum albumin and serum bilirubin (Child III, 1964), and the CYP activity was calculated based on the child-pugh score (El-Khateeb et al., 2021).

Table 3
Different strategies for opioid rotation from oral morphine to transdermal fentanyl.

No	1	2	3	4	5	6	7	8	9	10	11	12
Overlap time [h]	0	12	24	0	12	24	0	12	24	0	12	24
Nominal flux of 1st fentnayl patch [μg/h]	37.5	37.5	37.5	37.5	37.5	37.5	50	50	50	50	50	50
Nominal flux of 2nd fentnayl patch [μg/h]	37.5	37.5	37.5	50	50	50	37.5	37.5	37.5	50	50	50

mentioned in Section 2.1.1.1, we calculated the total plasma concentration of morphine, M6G, and M3G. The model was tailored according to the reported physiological features of the volunteers. The result of this validation is shown in Fig. 5, which represents the average experimental value for the 24 volunteers of Bochner et al. Study and simulated data by digital twin. Based on this result, the NRMSD for morphine, M6G, and M3G between the experimental data and simulated data is 0.44, 0.36, and 0.37, respectively. In addition, we calculated the area under the curve (AUC) for these three substances which are shown in Fig. 5.

3.2. Calibration of pharmacodynamics parameters for pain relief induced by morphine and its metabolites

The half-maximum effect concentrations for morphine, M6G, and M3G, based on Mazoit et al. study in 2007, are 124, 12.8, and 880 nM, respectively (Mazoit et al., 2007). In order to perform the validation for the pain prediction model for morphine therapy (Eq. (11)), we compared the calculated pain intensity based on the VAS scale to experimental pain score reports for immediate-release oral morphine in Christensen et al., 2008 study in 2018. In Christensen et al. Study, 45 healthy adult outpatients with average age of 20.6 years and 72.2 kg were chosen to undergo oral morphine therapy. 93 % of the volenteers were caucasians; 62 % were female; and their average height was 170.6 cm. As it is shown in Fig. 6, the average value of the pain intensity from the experimental data is shown in the blue line, and the calculated data by digital twin based on the Maziot et al. study is shown in the red line. As mentioned in Fig. 6, the NRMSD for immediate-release oral morphine is 0.51. Therefore, we performed our pain calculation for a wide range of values for half-maximum effect concentration ($\boldsymbol{IC}_{50,i}$) for morphine (50–300[nM]), M6G (5–100[nM]), and M3G (50–1000[nM]) and Hill coefficent (1–3). The optimization was performed by COMSOL Multiphysics Module, to reach the lowest NRMSD. Based on the result of this optimization, the $\boldsymbol{IC}_{50,i}$ for morphine, M3G, and M6G is 186.6, 111.6, and 26.1 [nM], respectively. The optimized value for the concentration

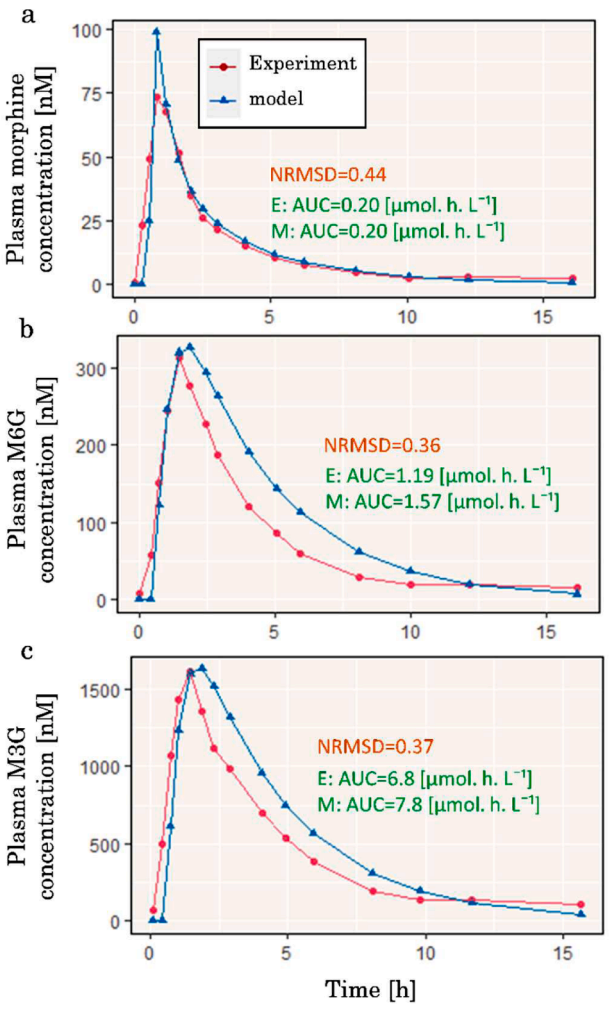

Fig. 5. Validation result for a: Morphine; b: M6G, and c: M3G total concentration in plasma produced by tailored digital twin compared to experimental data of Boncher et al. study on 1999 in 16 h by taking a 30.9 mg dose of immediate-release oral morphine.

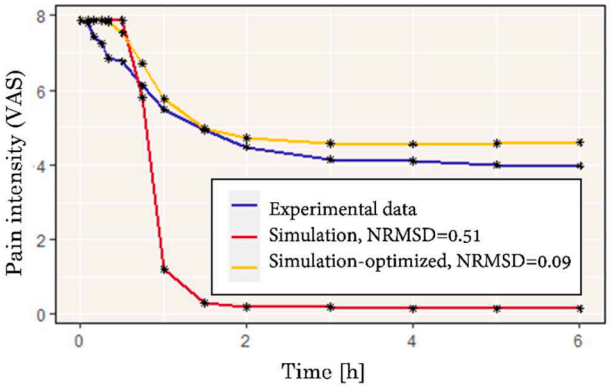

Fig. 6. The validation result for immediate-release oral morphine calculated values based on literature data and optimum values to fit the average pain intensity from the experimental data of Christensen et al. study in 2018.

of half-maximum effect for M3G is considerebly different from the reporetd value by Maziot et al. Study. This optimized value should be seen in the context of complex intraction of several parameters used in the optimization process. This value should be soley used in the combination of other optimized values for other parameters and it not neccessary a good repesentative for the real value of the concentration of the half-maximum effect for M3G. The Hill coefficient based on this optimization is equal to 1. The simulation results based on the optimum parameters are shown in Fig. 6 with a yellow line, which improved the NRMSD by 82 % compared to the values reported in the literature.

3.3. Validation for drug uptake, pharmacokinetics, and pharmacodynamics model for fentanyl transdermal therapy

An extensive exploration and study on validation of the drug uptake model of transdermal fentanyl drug delivery and its pharmacokinetics model were performed in our previous studies (Bahrami et al., 2022; Defraeye et al., 2020, 2021). Based on our previous studies, the normalized root-square-mean deviation (NRMSD) between our simulated fentanyl flux and experimental fentanyl flux (Rim et al., 2005) was 0.088 (Defraeye et al., 2021). Additionally, the fentanyl concentration calculated by the digital twin was validated against experimental data (Marier et al., 2006), which resulted in an NRMSD of 0.15 (Bahrami et al., 2022). The model parameters for the pain model for fentanyl were calibrated based on the experimental literature data (Sandler et al., 1992) by using the genetic algorithm as the optimization method, which led to the NRMSD of 0.09, and its details are provided in our previous study (Bahrami et al., 2022).

3.4. Oral morphine immediate-release followed by fentanyl transdermal therapy

Applying a similar treatment to patients with different physiological features and pathological states will lead to varied outcomes. In this section, we aimed to study the range of variability in outcomes of a similar treatment of oral morphine and transdermal fentanyl over the generated virtual population. The physics-based digital twin for immediate-release oral morphine followed by fentanyl transdermal therapy was tailored for 500 virtual patients, based on Tables 1 and 2. Each patient started therapy by taking 20 mg of immediate-release oral morphine and repeated it every 4 h. After 24 h, the first fentanyl patch with the nominal flux of 50 μg/h was applied, while for the next 12 h, taking immediate-release oral morphine was ongoing. Seventy-two hours after the first fentanyl patch, the old patch was removed, and the second fentanyl patch was applied. The whole process was monitored for 168 h (7 days). This therapy is based on conventional SmPC therapy in the clinics; the outcome of this therapy is shown in Fig. 7. The maximum concentration of the fraction of unbound morphine in plasma for virtual patients varies in a range of 27–61 nM. Based on the literature, the minimum effective concentration (MEC) for morphine is between 20 and 40 nM (Morphine Sulfate Injection, 2016), and all patients reach this threshold, as it is shown in Fig. 7a. The result for M6G and M3G fraction of unbound plasma concentration is shown in Fig. 7b and c, in which the maximum concentration of M6G varies between 106 and 425 nM and for M3G between 529 and 2127 nM. The fraction of unbound concentration of fentanyl in plasma is shown in Fig. 7d, in which the maximum fentanyl concentration after applying one patch varies between 1.1 and 2.5 ng/ml, while the therapeutic range of fentanyl concentration in plasma is between 0.6 and 3 ng/ml. As a result of morphine and fentanyl therapy, the pain intensity of the virtual patients drops; this result is shown in Fig. 7e. The minimum pain intensity during oral morphine therapy is between 3.2 and 4.4 VAS units; after the fentanyl patch, it is 0.5–3.3.

As we expected, the minimum pain intensity level took place during the placement of the first patch, as morphine, M6G, and fentanyl were present in the body. Patients with high pain intensity tend to have hyperventilation; as morphine or fentanyl therapy starts, the minute ventilation drops and this reduction can continue and even cause hypoventilation or, eventually, respiratory depression. Minute ventilation of virtual patients during the therapy is shown in Fig. 7f. The minimum of minute-ventilation during morphine therapy varies

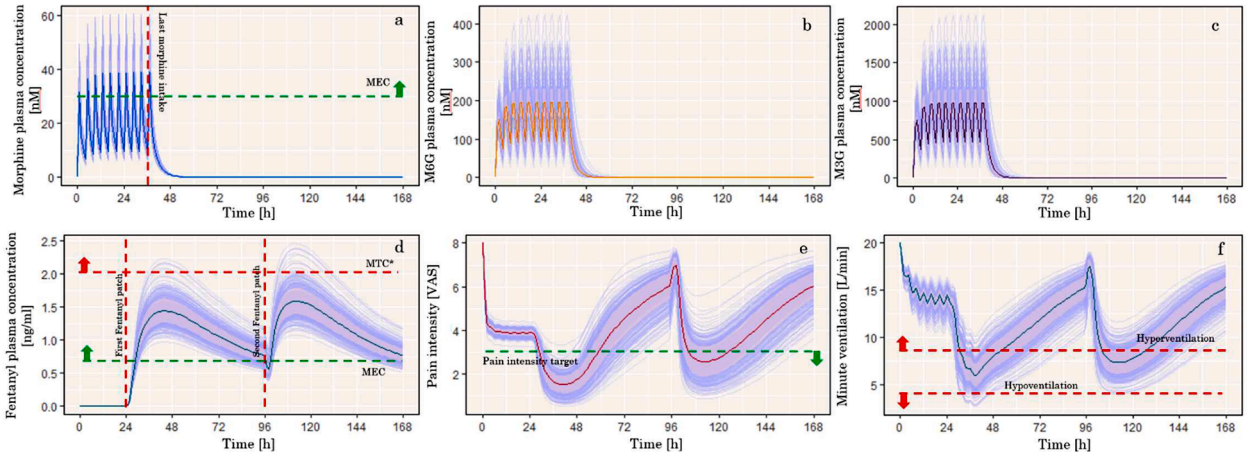

Fig. 7. a: morphine concentration in plasma (the green line represent the minimum effective concentration); b: M6G concentration in plasma; c: M3G concentration in plasma; d: fentanyl concentration in plasma (the green line represents the minimum effective concentration and the red line represents the minimum toxic concentration); e: pain intensity (the green line represent the higher target threshold for pain intensity); f: minute-ventilation (the upper red line represents the lower threshold for hyperventilation and the lower red in represents the upper threshold for hypoventilation), for the generated population over 168 h during oral immediate-release morphine therapy followed by Fentanyl transdermal therapy after 24 h from the start of the treatment. The shaded pink ribbon around the average line represented the variation of the result from the average by one standard deviation.

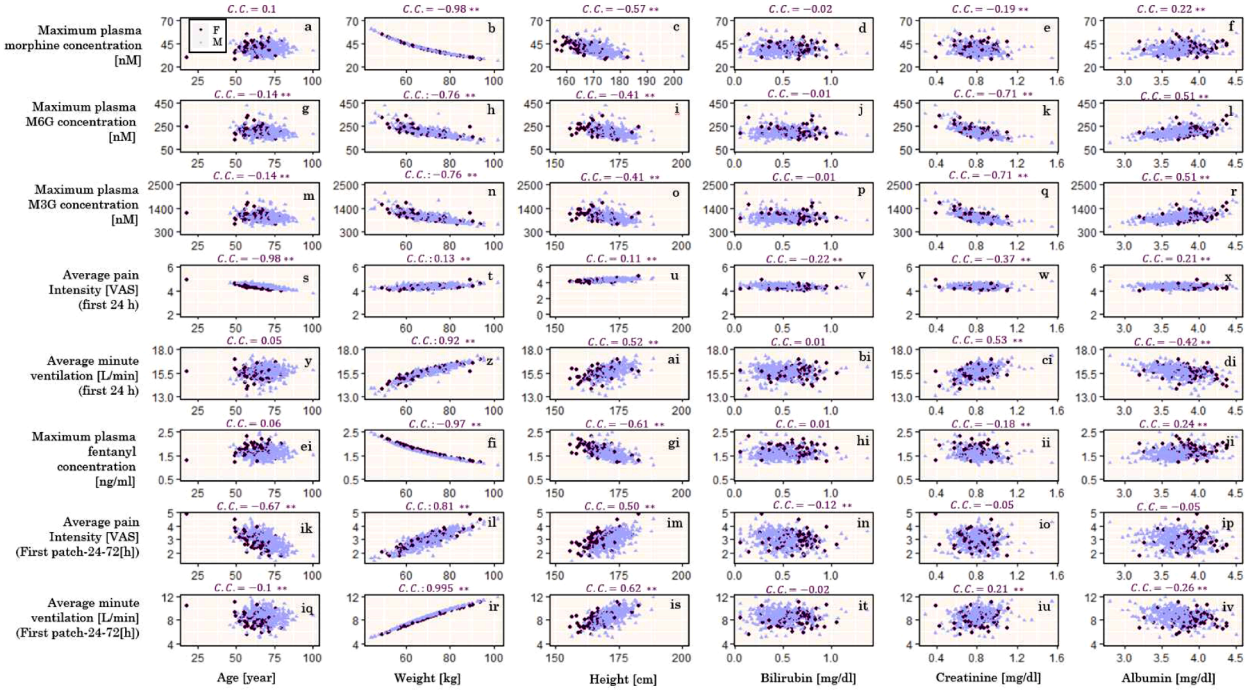

Fig. 8. a–f: maximum concentration of morphine in plasma; g–l: maximum concentration of M6G in plasma; m–r: maximum concentration of M3G in plasma; s–x: minimum pain intensity during the first 24 h; y, z, ai–di: minimum minute-ventilation during the first 24 h; ei–ji: the maximum concentration of fentanyl in plasma; i–ip: minimum pain intensity during last 72 h; iq–iv: minimum ventilation rate during last 72 h for virtual population based on the patient's physiology during oral immediate-release morphine therapy followed by Fentanyl transdermal therapy after 24 h from the start of the treatment.

between 10.4 and 15.6 L/min; during fentanyl transdermal therapy, it is between 2.7 and 10.1 L/min. Based on this result, the minute ventilation stays high during immediate-release oral morphine therapy; in the clinic, if the patient is still experiencing hyperventilation before switching the opioid, they try to adjust the morphine dose. However, in this study, we switched to fentanyl at the recommended time without changing the morphine therapy. However, after the first patch of fentanyl for some patients, it reaches hypoventilation, a sign of overdose, which some patients recover during the second patch of fentanyl. Based on this result, the same therapy for 500 virtual patients resulted in a widely spread outcome. The applied treatment meets the expectation of lowering the pain intensity and keeping the minute ventilation in the acceptable range while it fails to relieve the pain, or it reduces the minute ventilation drastically for the rest.

3.4.1. Impact of physiological features on oral morphine therapy followed by transdermal fentanyl therapy

Physiological features of the patients are one of the causes of variation in treatment outcomes. In this section, we explore the impact of each physiological feature on the main outcomes of the treatment. The

maximum concentration of unbound morphine in plasma corresponded to the patient's physiological features, as shown in Fig. 8a–f. Based on this result, the maximum concentration of morphine in plasma is very strongly correlated to weight (C.C.=-0.98) and moderately correlated to height (C.C.=-0.57); however, this correlation is weak (0.02–0.22) for the age serum bilirubin, creatinine, and albumin. As it is shown in Fig. 8g–r, the maximum concentration of M6G and M3G in plasma are strongly correlated to weight (C.C.=-0.76), and serum creatinine (C.C.=-0.71), and they are moderately correlated to height (C.C.=-0.41) and serum albumin (C.C.=0.51). The maximum concentration of M6G and M3G in plasma has a very weak correlation (0.01–0.14) with age and serum bilirubin. As it is shown in Fig. 8s–x, the average pain intensity during morphine therapy is very strongly correlated (C.C.=-0.98) to age and weakly correlated (0.21–0.37) to serum bilirubin, serum creatinine, and serum albumin. The correlation between pain intensity during morphine therapy and weight and height is very weak (0.11–0.13). The correlation between average minute ventilation during morphine therapy and physiological features is shown in Fig. 8y-di. Based on this result, the average minute ventilation strongly correlates (C.C.= 0.92) to weight and moderately (C.C.= 0.52) to height, serum creatinine, and serum albumin. The correlation between minute ventilation and age and serum bilirubin is very weak (0.01–0.05). As it is shown in Fig. 8ei–ji, maximum fentanyl plasma concentration is very strongly correlated (C.C.=-0.97) to weight and strongly correlated (C.C.=-0.61) to height. The correlation between maximum fentanyl concentration is weakly correlated (C.C.= 0.24) to albumin and very weakly correlated (0.01-0.18) to age, serum bilirubin, and serum creatinine. Also, the correlation between average pain intensity during the fentanyl transdermal therapy and physiological features is shown in Fig. 8ik–ip. The correlation between pain intensity and weight is very strong (C.C.= 0.81) and also strongly correlated (C.C.= −0.67) to age. Pain intensity during the fentanyl transdermal therapy and height are moderately correlated (C.C.= 0.50), while it is very weakly correlated (0.05–0.12) to serum bilirubin, serum creatinine, and serum albumin. As shown in Fig. 8iq–iv, the average minute ventilation during fentanyl transdermal therapy strongly correlates to weight and height (0.62–0.995). The average minute ventilation is weakly correlated (0.21–0.26) to serum creatinine and serum albumin and very weakly correlated (0.02–0.1) to age and serum bilirubin.

Based on this result, physiological features can drastically impact therapy outcomes, but the effect of these features is not the same. This result shows the impact of implementing the physiological features of the patient in order to have a more accurate insight into different aspects of opioid treatment. In oral morphine therapy, morphine concentration in plasma, its metabolites, and subsequently, the minute ventilation is highly correlated to the patient's weight. Additionally, M6G and M3G concentrations correlate to the serum creatinine and serum albumin concentration. However, the pain relief caused by oral morphine is strongly correlated with the age of the patient, and at higher ages, the pain relief is higher. Serum bilirubin did not have a big impact on the outcome of oral morphine therapy. During fentanyl transdermal therapy, the concentration of fentanyl in the plasma, pain intensity, and minute ventilation is highly correlated to the weight of the patient. Additionally, the pain intensity is also correlated to the age of the patient. Serum bilirubin, serum creatinine, and serum albumin had a low impact on the transdermal fentanyl therapy outcomes.

Alongside the treatment outcome that was studied in the previous paragraph, the duration of that patient's experience of mild pain during the treatment is one of the important parameters to evaluate the success of the treatment. VAS pain intensity three and lower is considered moderate pain; therefore, we aim to reach and stay in this range; we call this duration time without pain. This parameter represents the duration of comfort for the patient during the treatment. This section aimed to explore the impact of the physiological features on time without pain during oral morphine therapy, followed by transdermal fentanyl therapy. We examined the impact of physiological features on time without pain, and its result is shown in Fig. 9. The result shows a strong correlation between time without pain and age and the patient's weight. As age increases, the time without pain increases; however, as the patient's weight increases, the time without pain decreases. Height and time without pain have a moderate correlation; however, it should be noted that higher height is correlated with higher weight. The correlation between time without pain and serum bilirubin, serum creatinine, and serum albumin is very weak.

3.4.1.1. Sensitivity analysis of the physiological features. The result of the sensitivity analysis of minimum pain intensity over the physiological features is demonstrated in Fig. 10. Based on the result shown in Fig. 10a, the weight of the patient has the highest sensitivity index, followed by age and then creatinine. The sensitivity index of height, bilirubin, and albumin is up to 7.4 * 10^{-7}, 0, and 0 by considering 12 digits of accuracy, therefore, the sensitivity of minimum pain intensity on these features is negligible. At first sight, the low sensitivity index of height might look in contrast to the correlation coefficient of minimum pain intensity and height, however, it should be mentioned, in this case, the weight of the patient stays the same and does not change by the height, however, in the population, usually, the weight of the patients tend to be higher for higher heights. Additionally, the minimum pain

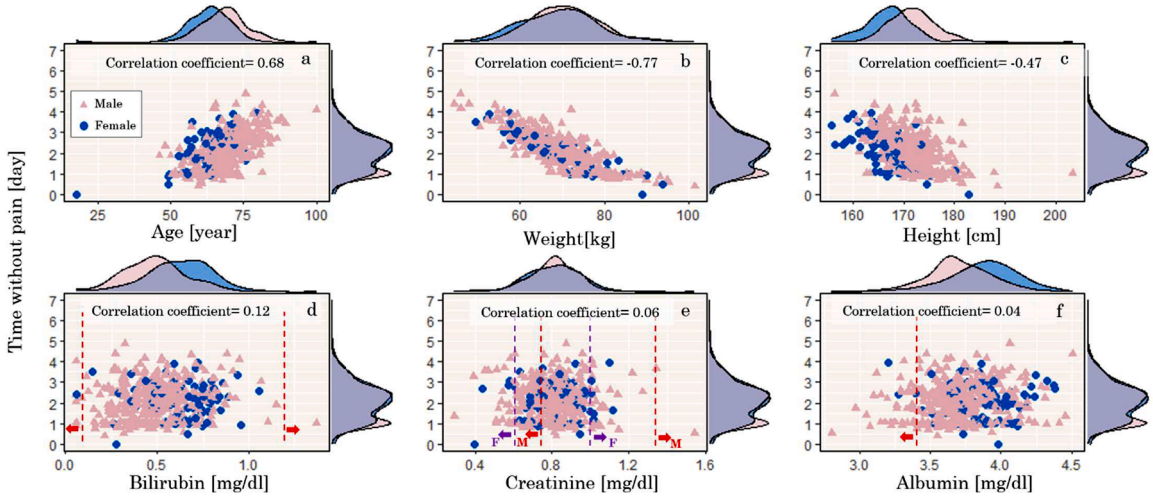

Fig. 9. Duration in which the patient experiences pain intensity below 3 on the VAS scale during 96 h of therapy started with immediate-release oral morphine followed by Fentanyl transdermal therapy after 24 h from the start of the treatment.

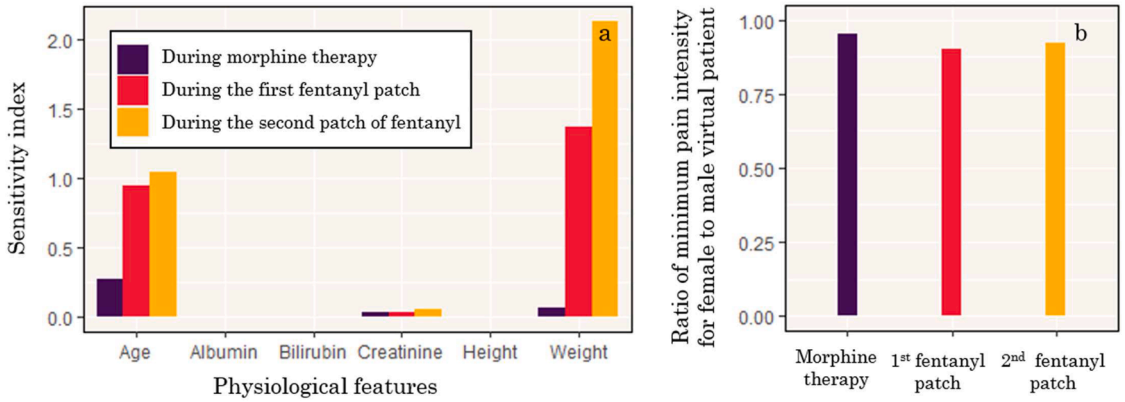

Fig. 10. a: sensitivity analysis results for the minimum pain intensity during oral morphine treatment, first fentanyl patch which overlaps for 12 h with oral morphine therapy, and second fentanyl patch; b: the ratio of minimum pain intensity when the virtual patient is female to when the virtual patient is male.

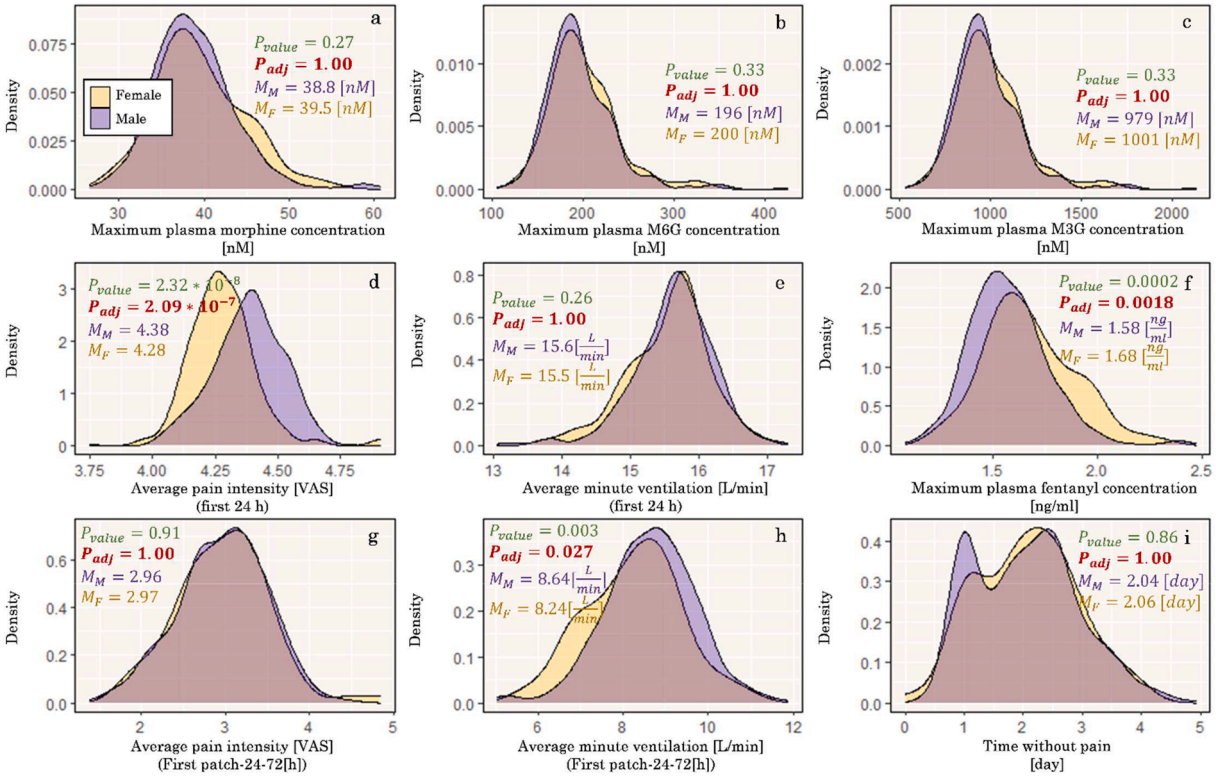

Fig. 11. Distribution of therapy outcomes, a: maximum plasma morphine concentration; b: maximum plasma M6G concentration; c: maximum plasma M3G concentration; d: average pain intensity during morphine therapy; e: average minute-ventilation; f: maximum plasma fentanyl concentration; g: average pain intensity during the first fentanyl patch; h: average minute-ventilation during the first fentanyl patch; and i: time without pain for both genders.

intensity during 2nd fentanyl patch is more sensitive to age, weight, and creatinine by 3.9, 30.6, and 1.8 folds. On the other hand, as shown in Fig. 10b, the minimum pain intensity for female virtual patients during morphine therapy, first fentanyl patch, and second fentanyl patch is 4.9 %, 9.7 %, and 7.7 % less than for male virtual patient. Based on these results, for the same condition, both in considered physiological features and treatment, the female virtual patient experiences less pain compared to the male virtual patient.

3.4.2. Impact of gender on oral morphine therapy followed by transdermal fentanyl therapy

We aim to identify to which extent the therapy is impacted by gender. To this end, we explored the distribution of treatment outcomes based on gender. As it is mentioned in Section 2.2.3, patient gender affects the model parameters. In order to evaluate the impact of gender on the outcome of therapy, we depicted the distribution of substances concentration in plasma pain intensity and minute ventilation for both genders in Fig. 11. As it is shown in Fig. 11a, the distribution of maximum morphine concentration is not significantly different for either gender ($p_{adj} = 1.00$, Adjusted p_{value} as a result of multiple comparision), and the difference between their means is 0.7 [nM]. The distribution of maximum M6G and M3G plasma concentrations per gender are shown in Fig. 11b, c, and there is no significant difference ($p_{adj} = 1.00$) between them. As it is shown in Fig. 11d, the distribution of minimum pain intensity during morphine therapy is significantly different ($p_{adj} = 2.088 * 10^{-7}$) for both genders, and there is a 0.10 unit of VAS pain intensity difference in their mean.

Based on the result in Fig. 11e, the distribution of average minute ventilation during morphine therapy is not significantly different for both genders. The distribution of maximum fentanyl concentration in plasma is significantly different ($p_{adj} = 0.0018$) for both genders, and there is a 0.1 [ng/ml] difference between their means, as shown in Fig. 11f. Based on the result in Fig. 11g, the minimum pain intensity for the first patch is not significantly different ($p_{adj} = 1.00$) regarding gender. As shown in Fig. 10h, the average minute ventilation is significantly different ($p_{adj} = 0.27$) for both genders, with a 0.4 [L/min] difference in their means. There is no significant difference in the time without pain either, as shown in Fig. 11i. Based on these results, the patient's gender significantly impacts fentanyl plasma concentrations and corresponding respiration as a result of fentanyl therapy; however, the impact of gender on therapy outcomes, such as morphine concentration in plasma or pain intensity, is negligible. As such, the proposed therapy should be strongly tailored to the gender of the patient to provide the best pain relief with minimal adverse effects.

3.5. *Exploring different strategies to rotate from oral morphine to fentanyl transdermal therapy*

In this section, we explore different strategies for switching from oral morphine to fentanyl to find which therapy best suits which group of patients. At the time of switching from oral morphine to transdermal fentanyl, the taking of oral morphine will continue for 12 h after the application of the first fentanyl patch, based on the protocol in the clinics. The size of the fentanyl patch is calculated based on different methods; by considering the 100:1 potency of fentanyl compared to morphine, they suggest the equivalent size of a fentanyl patch for 180 mg/ day of oral morphine (20 mg every 4 h) is the patch with the nominal flux of 50 μg/h (Donner et al., 1996). However, in other approaches, as suggested with Duragesic® fentanyl patches, the equivalent fentanyl patch for 180 mg/day of oral morphine is a fentanyl patch with a nominal flux of 37.5 μg/h (US Food and Drug Administration, 2005). We considered 12 different strategies, as combinations of 2 sizes of fentanyl patch (37.5 and 50 μg/h) and three different times for taking the last oral morphine. As the fentanyl therapy starts at 24 h, the overlap times are at 0 h, 12 h, and 24 h. These 12 strategies were applied to all 500 virtual patients, and these therapies' outcomes are shown in Fig. 12.

Based on Fig. 12a, as we expected, the average pain intensity reduces by increasing the overlap time or the dose of fentanyl. However, each strategy was successful for some groups of patients in keeping their pain intensity below the target. Based on the result shown in Fig. 12b, fentanyl therapy with 37.5 μg/h flux of fentanyl could not bring the minute ventilation to the comfort zone. However, for the patch with the nominal flux of 50 μg/h, the majority of the patient experienced a normal range of minute ventilation, while some patients had hypoventilation. Furthermore, we examined the fentanyl plasma concentration, and as is shown in Fig. 12c, by implementing a fentanyl patch with the nominal flux of 50 μg/h, some patients will have an average fentanyl concentration above 2 ng/ml. While considering the result in this section, we realized none of these therapies are successful for all patients regarding

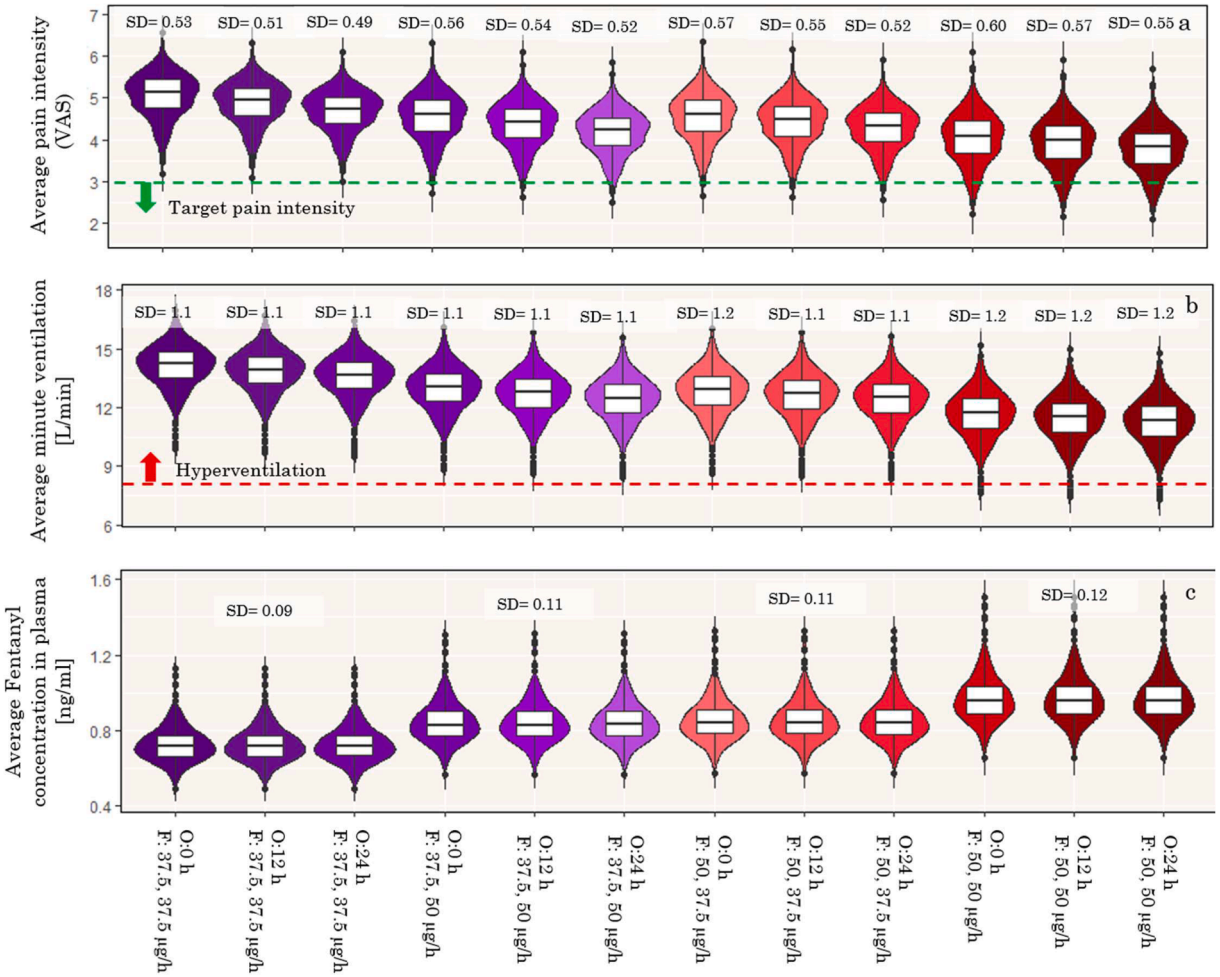

Fig. 12. a: average pain intensity, the green dashed line indicates the target pain intnesity; b: average minute ventilation, the red dashed line indicates the upper limit for normal minute ventilation; c: average fentanyl concentration in plasma for 12 different strategies of switching from oral morphine to transdermal fentanyl applied on 500 virtual patients during 168 h of therapy, starting from oral morphine followed by 2 fentanyl patches each with 72 h duration.

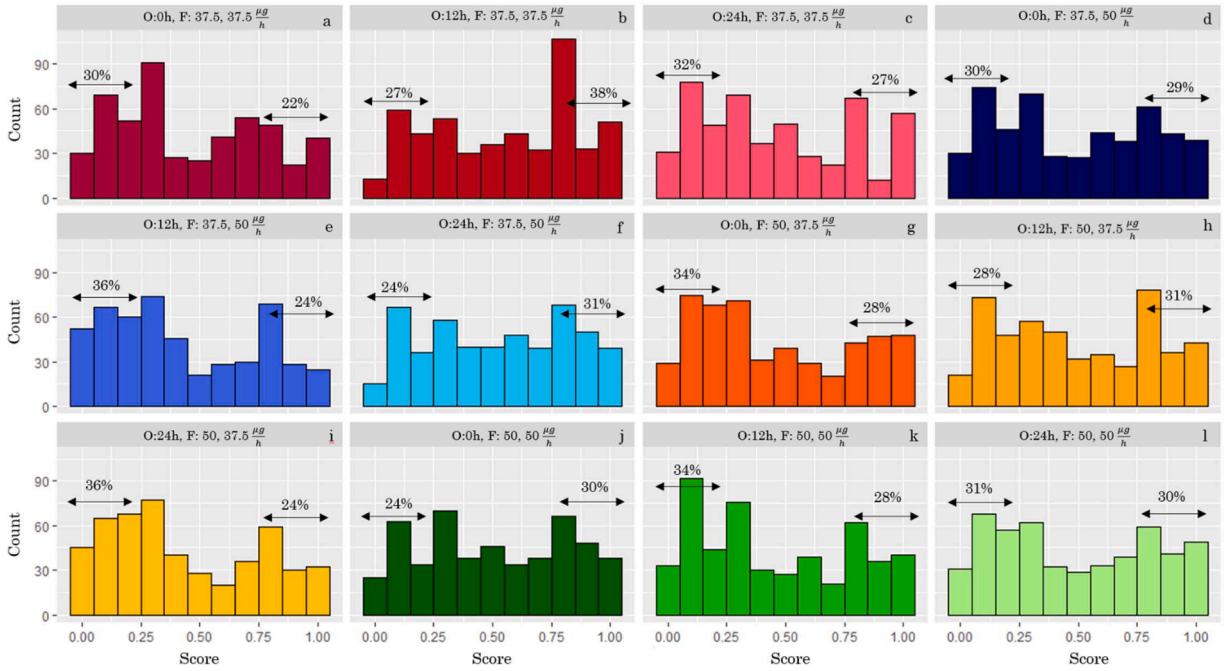

Fig. 13. Score of therapy with a: overlap time 0 h and first and second fentanyl patch of 37.5 μg/h; b: overlap time 12 h and first and second fentanyl patch of 37.5 μg/h; c: overlap time 24 h first and second fentanyl patch of 37.5 μg/h; d: overlap time 0 h and first fentanyl patch of 37.5 μg/h and second fentanyl patch of 50 μg/h; e: overlap time 12 h and first fentanyl patch of 37.5 μg/h and second fentanyl patch of 50 μg/h; f: overlap time 24 h and first fentanyl patch of 37.5 μg/h and second fentanyl patch of 50 μg/h; g: overlap time 0 h and first fentanyl patch of 50 μg/h and second fentanyl patch of 37.5 μg/h; h: overlap time 12 h and first fentanyl patch of 50 μg/h and second fentanyl patch of 37.5 μg/h; i: overlap time 24 h and first fentanyl patch of 50 μg/h and second fentanyl patch of 37.5 μg/h; j: overlap time 0 h and first and second fentanyl patch of 50 μg/h; k: overlap time 12 h and first and second fentanyl patch of 50 μg/h; l: overlap time 24 h and first and second fentanyl patch of 50 μg/h for the virtual patients.

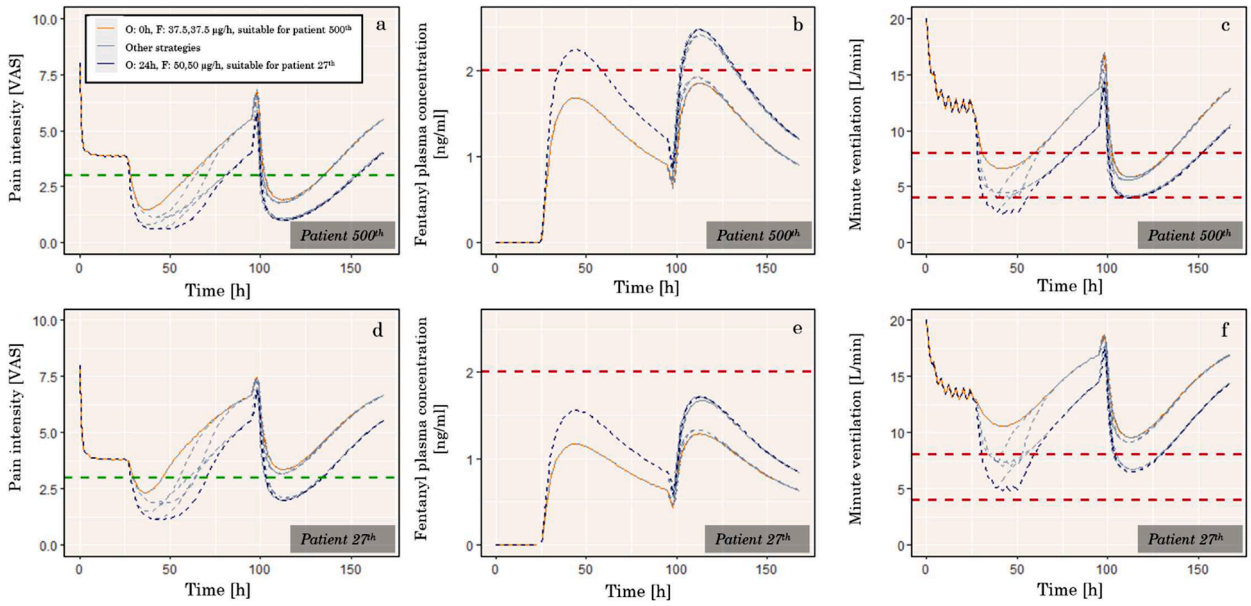

Fig. 14. a and d: pain intensity (the green line represents the pain intensity target); b and e:fentanyl plasma concentration (the red line represents the lower threshold for toxicity); c and f: minute ventilation (the area between the two red line represents the normal range of minute ventilation) during oral morphine therapy followed by two applications of transdermal fentanyl patch for the 500th and 27th of virtual patients.

pain relief efficiency and side effect safety. Therefore, it is necessary to choose a unique opioid rotation strategy for each virtual patient to meet the requirements.

In order to find which therapy best suits the virtual patient, we considered three outputs of opioid treatment; average pain intensity, average minute ventilation, and average fentanyl concentration in plasma to rank each strategy for each patient. Based on this ranking, the best strategy for each patient is chosen. The main criteria of the ranking were considered regarding pain intensity. To this end, the average pain intensity of 12 strategies was calculated for each patient and ranked lower to higher. The intensity of pain below three had a low impact on ranking, as below 3 was the target of the therapy. The average fentanyl

concentration below 2 ng/ml did not impact the ranking. However, the rank of the strategy was reduced if the maximum fentanyl concentration was above 2 ng/ml. Higher fentanyl concentration will increase the probability of side effects such as dizziness and nausea, which we did not consider directly in this study. On the other hand, as the minimum minute ventilation went above 8 L/min, the rank of the therapy was reduced; however, the reduction in the rank was higher if the minute ventilation was below 4 L/min. In this part, we considered hypoventilation a bigger downfall of therapy than hyperventilation. The result of this ranking is shown in Figs. 12,13.

In this result, a score equal to 1 represents the best therapy for virtual patient *i,* and the lowest score represents the worst therapy for virtual patient *i*. Based on the result shown in Figs. 12,13, each strategy is suitable for some groups of patients, while it fails to meet the criteria for other patients. In the next step, we look into the possibility of choosing the best strategy for the patient with a range of physiological features.

Due to different physiological features, the same opioid rotation strategy will lead to different outcomes for different patients. In Fig. 14 the outcomes of opioid therapy for the 27th and 500th virtual patient by considering different opioid rotation strategy is shown. Based on the outcome for the 500th virtual patient, the best suited opioid rotation strategies is the first strategy which was when the overlap time was 0 h and first and second fentanyl patch were with nominal flux of 37.5 μg/h. on the other hand for the 27th virtual patient, the twelfth strategy, with overlap time of 24 h and using fentanyl patches with nominal flux of 50 μg/h was the best suited opioid rotation strategy. Based on results in Fig. 14a–c, by applying the first strategy for the 500th virtual patient, the pain intensity reaches the target, the fentanyl concentration stays below the threshold, and the minute ventilation for the virtual patient is in the range of hyperventilation and normal range and no hypoventilation. However, the by applying the twelfth strategy on the 500th virtual patient we see, even though the pain intensity reaches the target, the fentanyl concentration goes beyond the threshold and throughout the treatment, the patient experiences hypoventilation. On the other side, for the 27th virtual patient, by the twelfth strategy the pain intensity is lower compared to time the when the first strategy is applied. And additionally, the twelfth strategy helps the minute ventilation of the 27th virtual patients reach the normal range. Based on this result, as mentioned earlier, one opioid strategy which is successful for one patient might fail to meet the requirement for the other patient.

3.5.1. Physiological features distribution of virtual patients based on their suitable opioid rotation strategy

We explored the deviation between the physiological features distribution of virtual patients based on their best-suited opioid rotation strategy. As is shown in Fig. 15a, c–g, there is a deviation in the distribution profile for these physiological features based on the best therapy for them; however, these differences are only more distinct for the patients' weight. The number of female virtual patients and male virtual patients in each subgroup pf the virtual patient based on best suited strategy is shown in Fig. 15b. For all the 12 strategies, as it is shown in Fig. 15b, females are 5 %, 38 %, 10 %, 15 %, 0 %, 20 %, 8 %, 14 %, 12.5 %, 10.5 %, 10 %, and 18 % of the patients. Among them, the therapies with two fentanyl patches with a nominal flux of 50 μg/h had the lowest percentage of females (5 %), which means this therapy was more suitable for males than females. On the other hand, the therapy with the combination of fentanyl patches with the nominal flux of 50 and 37.5 μg/h and overlap time of 24 h has the highest percentage of females (31.2 %). By considering this percentage and the percentage of females in the generated population (16.2 %), we realized the treatment with nominal fentanyl flux of 50 and 37.5 μg/h and 24 h overlap was the most suitable therapy for females. The combined distribution of physiological features based on the best suited therapy is provided in the supplementary material.

4. Outlook

In this study, the developed physics-based digital twin was tailored to the patient's age, weight, gender, height, serum bilirubin, serum creatinine, and serum albumin. The digital twin was used to explore the impact of physiological features on opioid rotation from oral morphine to transdermal fentanyl. In order to improve the accuracy of the model and bring it closer to reality, here are a few suggestions:

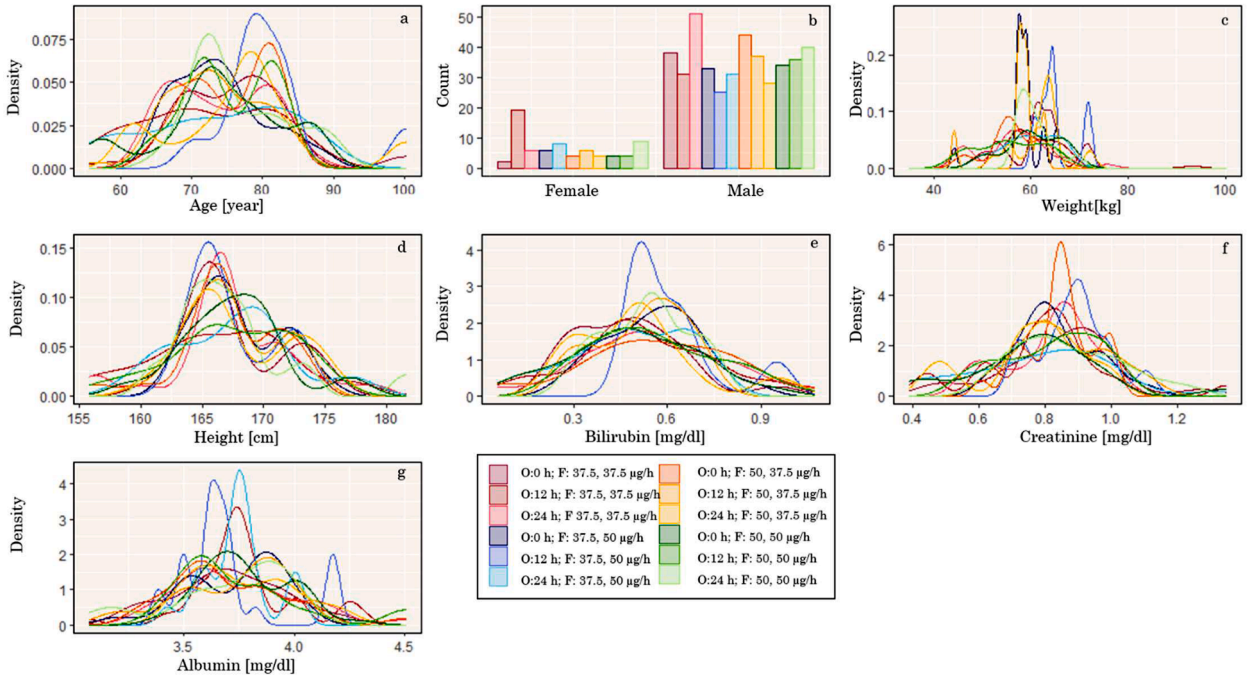

Fig. 15. Distribution of a: age; b: the number of female virtual patient and male patient in each subgroup of the population; c: weight; d: height; e: serum bilirubin; f: serum creatinine; and g: serum albumin of the virtual patients divided based on the best therapies for them.

- It is important to evaluate the performance of tailored digital twins in the clinic. Therefore, a clinical validation study in which the digital twin is tailored to a specific patient to predict individual fentanyl transdermal doses from stable oral morphine therapy switch.
- The morphine therapy prior to the fentanyl switch is administrated in different ways, such as subcutaneous, immediate-release oral, and controlled-release oral. Therefore, exploring other administration routes of morphine therapy will provide more insight into opioid rotation.
- We only considered seven physiological features in this study due to the lack of further data. However, taking into account other physiological features and states, including skin properties, will improve the tailoring of digital twins.

5. Conclusions

In this study, we developed a tailored physics-based digital twin to simulate the switch from immediate-release oral morphine to transdermal fentanyl in cancer patients. Our aim was to explore the impact of individual patient parameters on immediate-release oral morphine, transdermal fentanyl, and switching from oral morphine to transdermal fentanyl. Based on the results, the maximum concentration of morphine in plasma varied between 26 and 61 nM, and the maximum concentration of fentanyl varied between 1.1 and 2.5 ng/ml for all the virtual patients undergoing the same approach and dose of fentanyl and morphine therapy. This high variation in plasma concentration for morphine and fentanyl among the virtual patients led to high variability in the effect of therapy, such as pain relief and reduction in minute ventilation, which the dosing in this therapy was not modified based on individual pain experience. During these seven days of treatment, the time without pain varied from one day to almost seven days for the virtual patients. Therefore, this therapy, which is not tailored for individual patients, was successful for a specific group, while it failed to meet the treatment requirements for the rest. This result emphasizes the importance of individualizing the patients' treatment to control the pain while avoiding overdosing.

To this end, we explored 12 strategies by changing the overlap of oral morphine and fentanyl transdermal therapy and the subsequent fentanyl patch dose. According to the outcome of the therapy, each strategy was suitable for a specific group of patients, while it failed for the rest. Based on this result, we conclude that different patients, in addition to different morphine and fentanyl therapy, need different opioid-rotation in order to have sufficient pain relief while not experiencing too disturbing or dangerous side effects. Furthermore, the physiological feature distribution of the virtual patients was studied based on their best-suited strategy. This result showed that only one or two physiological feature is insufficient for strategy selection. It is important to consider all the physiological features that impact oral morphine and transdermal fentanyl therapy.

CRediT authorship contribution statement

Flora Bahrami: Conceptualization, Data curation, Formal analysis, Methodology, Software, Validation, Visualization, Writing – original draft, Writing – review & editing. **René Michel Rossi:** Writing – review & editing. **Katelijne De Nys:** Conceptualization, Writing – review & editing. **Markus Joerger:** Conceptualization, Writing – review & editing. **Milena Cukic Radenkovic:** Writing – original draft. **Thijs Defraeye:** Conceptualization, Funding acquisition, Project administration, Supervision, Writing – review & editing.

Data availability

Data will be made available on request.

Acknowledgments

This work was financially supported by OPO Foundation (grant "Digital human avatars help tailor transdermal pain management (TREATME)"), and the Margrit Weisheit Foundation and the Parrotia Foundation (grant "Digitale menschliche Avatare helfen bei der Anpassung der transdermalen Schmerztherapie in Echtzeit"). The funders were not involved in the study design, collection, analysis, and interpretation of data, the writing of this article, or the decision to submit it for publication.

Supplementary materials

Supplementary material associated with this article can be found, in the online version, at doi:10.1016/j.ejps.2024.106727.

References

Bahrami, F., Rossi, R.M., De Nys, K., Defraeye, T., 2023. An individualized digital twin of a patient for transdermal fentanyl therapy for chronic pain management. Drug Deliv. Transl. Res. 13, 1–14.

Bahrami, F., Rossi, R.M., Defraeye, T., 2022. Predicting transdermal fentanyl delivery using physics-based simulations for tailored therapy based on the age. Drug Deliv. 29 (1), 950–969. https://doi.org/10.1080/10717544.2022.2050846.

Bisaso, K.R., Mukonzo, J.K., Ette, E.I., 2022. Stimulus–Response mechanistic modeling of pharmacodynamic drug-drug interaction: extension of the operational receptor model of agonism. Inform. Med. Unlocked 28, 100813.

Björkman, S., 2003. Reduction and lumping of physiologically based pharmacokinetic models: prediction of the disposition of fentanyl and pethidine in humans by successively simplified models. J. Pharmacokinet. Pharmacodyn. 30 (4), 285–307. https://doi.org/10.1023/A:1026194618660.

Bjorkman, S., Wada, R.D., Stanski, D., 1998. Application of physiologic models to predict the influence of changes in body composition and blood flows on the pharmacokinetics of fentanyl and alfentanil in patients. Anesthesiology 88 (3), 657–667. The Journal of the American Society of Anesthesiologists.

Bochner, F., Somogyi, A.A., Christrup, L.L., Larsen, U., Danz, C., Elbaek, K., 1999. Comparative pharmacokinetics of two modified-release oral morphine formulations (Reliadol® and Kapanol®) and an immediate-release morphine tablet (Morfin 'DAK') in healthy volunteers. Clin. Drug Investig. 17, 59–66.

Boireau-Adamezyk, E., Baillet-Guffroy, A., Stamatas, G.N., 2014. Age-dependent changes in stratum corneum barrier function. Skin Res. Technol. 20 (4), 409–415. https://doi.org/10.1111/srt.12132.

Christensen, K.S., Cohen, A.E., Mermelstein, F.H., Hamilton, D.A., McNicol, E., Babul, N., Carr, D.B., 2008. The analgesic efficacy and safety of a novel intranasal morphine formulation (morphine plus chitosan), immediate release oral morphine, intravenous morphine, and placebo in a postsurgical dental pain model. Anesth. Analg. 107 (6), 2018–2024.

de Bruijn, P., Kuip, E.J.M., Lam, M., Mathijssen, R.H.J., Koolen, S.L.W., 2018. Journal of Pharmaceutical and Biomedical Analysis Bioanalytical methods for the quantification of hydromorphone, fentanyl, norfentanyl, morphine, morphine-3ß-glucuronide and morphine-6ß-glucuronide in human plasma. J. Pharm. Biomed. Anal. 149, 475–481. https://doi.org/10.1016/j.jpba.2017.11.035.

Child III, C.G., 1964. Surgery and portal hypertension. The Liver and Portal Hypertension. Saunders, Philadelphia.

Eastern Metropolitan Region Palliative Care Consortium (2014). Opioid conversion ratios–Guide to practice 2010.

Corli, O., Roberto, A., Corsi, N., Galli, F., Pizzuto, M., 2019. Opioid switching and variability in response in pain cancer patients. Supportive Care in Cancer 27, 2321–2327.

De Gregori, S., De Gregori, M., Ranzani, G.N., Allegri, M., Minella, C., Regazzi, M., 2012. Morphine metabolism, transport and brain disposition. Metabolic brain disease 27, 1–5.

Defraeye, T., Bahrami, F., Ding, L., Malini, R.I., Terrier, A., Rossi, R.M., 2020. Predicting transdermal fentanyl delivery using mechanistic simulations for tailored therapy. Front. Pharmacol. 11, 585393.

Defraeye, T., Bahrami, F., Rossi, R.M., 2021. Inverse mechanistic modeling of transdermal drug delivery for fast identification of optimal model parameters. Front. Pharmacol. 12, 442.

Derraik, J.G.B., Rademaker, M., Cutfield, W.S., Pinto, T.E., Tregurtha, S., Faherty, A., Hofman, P.L., 2014. Effects of age, gender, BMI, and anatomical site on skin thickness in children and adults with diabetes. PLoS One 9 (1), 1–6. https://doi.org/10.1371/journal.pone.0086637.

Doherty, M.M., Poon, K., Tsang, C., Pang, K.S., 2006. Transport is not rate-limiting in morphine glucuronidation in the single-pass perfused rat liver preparation. J. Pharmacol. Exp. Ther. 317 (2), 890–900.

Donner, B., Zenz, M., Tryba, M., Strumpf, M., 1996. Direct conversion from oral morphine to transdermal fentanyl: a multicenter study in patients with cancer pain. Pain 64 (3), 527–534. https://doi.org/10.1016/0304-3959(95)00180-8.

Drug Enforcement Administration (DEA), U.S. Department of Justice, 2007. Control of a chemical precursor used in the illicit manufacture of fentanyl as a List I chemical. Interim rule with request for comments. Fed. Regist. 72 (77), 20039–20047.

El-Khateeb, E., Darwich, A.S., Achour, B., Athwal, V., Rostami-Hodjegan, A., 2021. Time to revisit Child-Pugh score as the basis for predicting drug clearance in hepatic impairment. Aliment. Pharmacol. Ther. 54 (4), 388–401.

Encinas, E., Calvo, R., Lukas, J.C., Vozmediano, V., Rodriguez, M., Suarez, E., 2013. A predictive pharmacokinetic/pharmacodynamic model of fentanyl for analgesia/sedation in neonates based on a semi-physiologic approach. Pediatr. Drugs 15 (3), 247–257. https://doi.org/10.1007/s40272-013-0029-1.

Felmlee, M.A., Morris, M.E., Mager, D.E., 2012. Mechanism-based pharmacodynamic modeling. Comput. Toxicol. I, 583–600.

Firooz, A., Rajabi-Estarabadi, A., Zartab, H., Pazhohi, N., Fanian, F., Janani, L., 2017. The influence of gender and age on the thickness and echo-density of skin. Skin Res. Technol. 23 (1), 13–20. https://doi.org/10.1111/srt.12294.

German, C., 2019. Computational framework for predictive PBPK-PD-Tox simulations of opioids and antidotes. J. Pharmacokinet. Pharmacodyn. 46 (6), 513–529. https://doi.org/10.1007/s10928-019-09648-1.

Holmberg, K., Kong, J., Lee, S., & Horwitz, J. (2008). The effects of applied local heat on transdermal drug delivery systems.

Giannos, T., Lesnik, S., Bren, U., Hodoscek, M., Domratcheva, T., Bondar, A.N., 2021. CHARMM force-field parameters for morphine, heroin, and oliceridine, and conformational dynamics of opioid drugs. J. Chem. Inf. Model. 61 (8), 3964–3977.

Imaoka, T., Huang, W., Shum, S., Hailey, D.W., Chang, S.Y., Chapron, A., Kelly, E.J., 2021. Bridging the gap between *in silico* and *in vivo* by modeling opioid disposition in a kidney proximal tubule microphysiological system. Sci. Rep. 11 (1), 21356.

Jackson, L.D., Wortzman, R., Chua, D., Selby, D., 2021. Opioid rotation from transdermal fentanyl to continuous subcutaneous hydromorphone in a cachectic patient: A case report and review of the literature. J. Oncol. Pharm. Pract. 27 (1), 238–243.

Juul, R.V., Nyberg, J., Lund, T.M., Rasmussen, S., Kreilgaard, M., Christrup, L.L., Simonsson, U.S.H., 2016. A pharmacokinetic-pharmacodynamic model of morphine exposure and subsequent morphine consumption in postoperative pain. Pharm. Res. 33, 1093–1103.

Macintyre, P.E., Jarvis, D.A., 1996. Age is the best predictor of postoperative morphine requirements. Pain 64 (2), 357–364.

Manitz, R., Lucht, W., Strehmel, K., Weiner, R., Neubert, R., 1998. On mathematical modeling of dermal and transdermal drug delivery. J. Pharm. Sci. 87 (7), 873–879. https://doi.org/10.1021/js970329r.

Marier, J.F., Lor, M., Potvin, D., DiMarco, M., Morelli, G., Sædder, E.A., 2006. Pharmacokinetics, tolerability, and performance of a novel matrix transdermal delivery system of fentanyl relative to the commercially available reservoir formulation in healthy subjects. J. Clin. Pharmacol. 46 (6), 642–653. https://doi.org/10.1177/0091270006286901.

Martini, C., Olofsen, E., Yassen, A., Aarts, L., Dahan, A., 2011. Pharmacokinetic-pharmacodynamic modeling in acute and chronic pain: an overview of the recent literature. Expert Rev. Clin. Pharmacol. 4 (6), 719–728. https://doi.org/10.1586/ecp.11.59.

Mazoit, J.X., Butscher, K., Samii, K., 2007. Morphine in postoperative patients: pharmacokinetics and pharmacodynamics of metabolites. Anesth. Analg. 105 (1), 70–78.

Mercadante, S., Adile, C., Ferrera, P., Grassi, Y., Cascio, A.L., Casuccio, A., 2023. Conversion ratios for opioid switching: a pragmatic study. Supportive Care in Cancer 31 (1), 91.

Miller, R.S., Peterson, G.M., McLean, S., Möller, C., 1997. Effect of cardiopulmonary bypass on the plasma concentrations of fentanyl and alcuronium. J. Clin. Pharm. Ther. 22 (3), 197–205. https://doi.org/10.1046/j.1365-2710.1997.94875948.x.

Money, S., Garber, B., 2018. Management of cancer pain. Current Emergency and Hospital Medicine Reports 6, 141–146.

Morphine Sulfate Injection, 2016. USP 1–27.

Oosten, A.W., Abrantes, J.A., Jönsson, S., Matic, M., van Schaik, R.H.N., de Bruijn, P., Mathijssen, R.H.J., 2017. A prospective population pharmacokinetic study on morphine metabolism in cancer patients. Clin.Pharmacokinet. 56, 733–746.

Paice, J.A., Ferrell, B., 2011. The management of cancer pain. CA Cancer J. Clin. 61 (3), 157–182.

Pauli-Magnus, C., Hofmann, U., Mikus, G., Kuhlmann, U., Mettang, T., 1999. Pharmacokinetics of morphine and its glucuronides following intravenous administration of morphine in patients undergoing continuous ambulatory peritoneal dialysis. Nephrol. Dial. Transplant. 14 (4), 903–909. Official Publication of the European Dialysis and Transplant Association-European Renal Association.

Periasamy, S., Poovathai, R., Pondiyadanar, S., 2014. Influences of gender on postoperative morphine consumption. J. Clin. Diagn. Res. JCDR 8 (12), GC04.

Rennick, A., Atkinson, T., Cimino, N.M., Strassels, S.A., McPherson, M.L., Fudin, J., 2016. Variability in opioid equivalence calculations. Pain medicine 17 (5), 892–898.

Podlewska, S., Bugno, R., Kudla, L., Bojarski, A.J., Przewlocki, R., 2020. Molecular modeling of μ opioid receptor ligands with various functional properties: PZM21, SR-17018, morphine, and fentanyl—simulated interaction patterns confronted with experimental data. Molecules 25 (20), 4636.

Ricarte, A., Dalton, J.A., Giraldo, J., 2021. Structural assessment of agonist efficacy in the μ-opioid receptor: morphine and fentanyl elicit different activation patterns. Journal of Chemical Information and Modeling 61 (3), 1251–1274.

Rim, J.E., Pinsky, P.M., Van Osdol, W.W., 2005. Finite element modeling of coupled diffusion with partitioning in transdermal drug delivery. Ann. Biomed. Eng. 33 (10), 1422–1438. https://doi.org/10.1007/s10439-005-5788-6.

Robert, L., Labat-Robert, J., Robert, A.-M., 2012. Physiology of Skin Aging. Clin. Plast. Surg. 39 (1), 1–8.

Sandler, A.N., Stringer, D., Panos, L., Badner, N., Friedlander, M., Koren, G., Klein, J., 1992. A randomized double-blind comparison of lumbar epidural and intravenous fentanyl infusions for postthoracotomy pain relief. Anesthesiology 77, 626–634.

US Food and Drug Administration. (2005). Duragesic Label.

Treillet, E., Laurent, S., Hadjiat, Y., 2018. Practical management of opioid rotation and equianalgesia. Journal of pain research 2587–2601.

Yassen, A., Olofsen, E., Romberg, R., Sarton, E., Teppema, L., Danhof, M., Dahan, A., 2007. Mechanism-based PK/PD modeling of the respiratory depressant effect of buprenorphine and fentanyl in healthy volunteers. Clin. Pharmacol. Ther. 81 (1), 50–58. https://doi.org/10.1038/sj.clpt.6100025.